The postcranium of the carnivorous cynodont *Chiniquodon* from the Middle Triassic of Namibia and the palaeo-environment of the Upper Omingonde Formation

Helke Brigitte Mocke

A Dissertation submitted to the Faculty of Science, University of the Witwatersrand, in fulfilment of the requirements for the Degree of Master of Science

Johannesburg, 2015

Declaration

I declare that this thesis is my own, unaided work, except where specific acknowledgement is made to the work of others. It is being submitted for the Degree of Master of Science at the University of the Witwatersrand, Johannesburg, and has not been submitted before for any degree or examination at any other university.

18 day of June 2015

I would like to dedicate this thesis to my parents,

who have inspired me throughout my growing up years

to always follow my passion.

†Hartmut Sören Wagner

Bridget Ann Wagner

Abstract

The Chiniquodontidae is a family of Triassic carnivorous cynodonts well represented in the Middle-Upper Triassic of Argentina and Brazil. Chiniquodontids were more recently discovered in Madagascar and central Namibia, representing the only record of the family outside South America. The Namibian specimen was discovered in the Upper Omingonde Formation and is represented by the skull and a partial skeleton. The new chiniquodontid was identified as *Chiniquodon* and is diagnosed by the postcranial characteristics identified; a strong bend in the proximal portion of thoracic ribs, reduced curvature of the clavicle, although this may be due to deformation, robustness of the neck of the ilium, differences in the angulation between the edge of the posterior lamina of the ilium and the margin of the neck, and a large ischium, which is more than twice the size of the pubic plate. The postcranial material of the chiniquodontid from Namibia is described and compared with that of South American chiniquodontids. Chiniquodontids lack costal plates on ribs, show a tall and slender scapular blade, a large acromion process positioned well above the scapular neck and absence of disc-like phalanges in the autopodium. The Namibian *Chiniquodon* provides the first evidence of elements from the pes in chiniquodontids, and one of the few for non-mammaliaform cynodonts. Sedimentological studies confirm that the Upper Omingonde Formation of Namibia represents fluvial deposits of braided and meandering rivers formed in a predominately arid climatic regime during the Middle Triassic.

Acknowledgements

I would like to thank the Federal Institute for Geosciences and Natural Resources (BGR) for funding this research, and Mr L. Feldhaus, Dr M. Quinger and Ms A. Lüttig for administrative assistance during my research. I would also like to thank the following individuals, who have contributed to the successful completion of this thesis: Professor Fernando Abdala from the University of the Witwatersrand, Evolutionary Studies Institute (ESI), for continual mentorship and guidance during this research; Dr Ansgar Wanke from the University of Namibia (UNAM), Geology Department, for mentorship and guidance of the geological component of my thesis; Dr Roger Swart for mentorship, help with field work and valuable comments on the geology; Dr G.I.C. Schneider, Director of the Geological Survey of Namibia (GSN), for granting permission to do this research and for comments on the geology; Dr Zubair Jinnah from the Witwatersrand University, Geology Department, for valuable comments on the geology as well as providing access to a microscope for petrographic descriptions; Dr P. Schreck for providing valuable tips on petrography; the National Heritage Council of Namibia (NHC) for granting a permit to export the *Chiniquodon* fossil to the ESI for study; Ms Jessica Cundiff for access to the chiniquodontids in the Museum for Comparative Zoology (MCZ) collections, University of Harvard, Boston Massachusetts; Mr T. Nemavhundi from the ESI, for preparing the *Chiniquodon* fossil; Mr I. Hlahane (GSN, labs) for producing geological thin sections and Mr P. Shigwedha (GSN, cartography) for producing geology section diagrams. Finally, I would like to express my sincere gratitude to Mr and Mrs Sorahda for permission to work on their Farm Okawaka; Mr Amoni Victor for allowing access on his Farm Omingonde and Mr Reinhold Strobel from Farm Otjihaenamaperero, for guidance and hospitality. Finally, I would like to express my sincere thanks to my family, especially my mother and husband, friends and colleagues, for their patience and encouragement during the time spent working on this thesis.

Table of Contents

List of Figures

List of Tables

List of Appendices

1. Chapter One

1.1. Introduction

The Triassic, 250 to 210 million years ago, is an interesting time in Earth's history, as many terrestrial vertebrate groups, like mammaliaforms (early mammals of some scholars) and dinosaurs make their first appearance (Erickson, 2002). Extensive studies have been done on Triassic palaeo-geography (e.g. Smith, 1999; Veevers, 2004), stratigraphy and sedimentary environments (e.g. Smith *et al.*, 1993; Holzförster *et al.* 1999; Rogers *et al.*, 2001; Zerfass *et al.*, 2003), biostratigraphy (Rubidge, 1995; Lucas, 1998) and the extinction events that occurred during the beginning and the end of the Triassic (e.g. Erwin, 1990; Ward *et al.*, 2000; Tanner *et al.*, 2001; Benton and Twitchett, 2003; Retallack *et al.*, 2006; Blackburn *et al.*, 2013). The Triassic started with a huge super-continent called Pangaea and ended with its break-up into Laurasia in the north and Gondwana in the south (Erickson, 2002). A large ocean, the Tethys, separated Eurasia from Gondwanaland, opening eastwards into the ancestral Pacific (Tucker and Benton, 1982).

Climatic interpretations indicate that conditions were changing from extremely cold at the beginning of the Triassic to very hot and arid at the end of the period (Catuneanu *et al.*, 2005). According to Tucker and Benton (1982), these conditions arose from the unique arrangement of continent and ocean at this time, with a) continentality effects more pronounced, including hot summers, cool winters and lower rainfall, as a result of the existence of one large landmass and b) more efficient heat transfer from low latitudes to the poles, due to the presence of a vast open ocean.

The non-mammaliaform cynodonts are a group of advanced therapsid fossils, which lived from the Permian to the Cretaceous. From an evolutionary point of view, they are important because representatives of this group gave rise to mammaliaforms during the Late Triassic (Hopson and Kitching, 1972; Kielan-Jaworowska *et al.*, 2004; Kemp, 2005), by which time

they were living on nearly all the continents (Rubidge and Sidor, 2001; Kemp, 2005; Abdala and Ribeiro, 2010).

The Chiniquodontidae is a family of small to large carnivorous cynodonts, having a secondary palate extending to or beyond the posterior end of the tooth row, and with sectorial teeth with small or no cingulum cusps, or teeth with broad lingual shelves contacting in occluding teeth (Hopson and Kitching, 1972, but see Abdala and Giannini, 2002). They form part of the clade Probainognathia (Hopson and Kitching, 2001), which gave rise to mammals. Von Huene (1936) erected the Family Chiniquodontidae, after the discovery of two species, *Chiniquodon theotonicus* and *Belesodon magnificus*, in outcrops of the Santa Maria Formation at Chiniquá, Rio Grande do Sul, Brazil. However, he did not give a full diagnosis of the family as the specimens used were a fragmentary skull (*Chiniquodon*) or a poorly preserved partial skeleton, including a very deformed skull (*Belesodon*).

Bonaparte (1966) described a series of highly fragmented *Chiniquodon* specimens from the Ischigualasto Formation of Argentina, whereas Romer (1969a) described poorly preserved skulls of *Chiniquodon* and *Belesodon* from the Santa Maria Formation, Brazil. Other taxa were added to the family, including *Probelesodon lewisi* and *Probelesodon minor* both from the Chañares Formation of Argentina (Romer, 1969b; Romer, 1973), *Probelesodon kitchingi* from the Santa Maria Formation, Rio Grande do Sul, Brazil (Teixeira, 1982), and *Probelesodon sanjuanensis* from the Ischigualasto Formation, Argentina (Martinez and Forster, 1996).

Abdala and Giannini (2002) performed a taxonomic revision of the Chiniquodontidae and an allometric study of the specimens included in the family based on cranial measurements. They proposed two autapomorphies as characteristic of the group: 1) the distinctive angulation between the posterior portion of the maxilla and the anterior position of the

zygomatic arch and; 2) very extended pterygoid flanges, ending in a thin projection. These authors confine the family to two taxa: *Chiniquodon theotonicus* and *Chiniquodon sanjuanensis*. Abdala and Giannini (2002) excluded the African taxon *Aleodon brachyramphus* from the Family Chiniquodontidae, a conclusion not endorsed by Hopson and Kitching (2001).

During the 1970s, a South African palaeontologist, Andre Keyser, discovered several fossils at various stratigraphic levels of the Omingonde Formation of central Namibia. These included the dicynodonts *Kannemeyeria* and *Dolichuranus*, the bauriid therocephalian *Herpetogale*, an eriopoid amphibian resembling *Micropholis* and the cynodonts, *Cynognathus*, *Trirachodon* and *Diademodon* (Keyser, 1973a, b; Keyser, 1978). Based on the discovery of this fossil fauna, the Omingonde Formation was interpreted as having an Olenekian-Anisian age (Kitching, 1995).

Until recently, *Chiniquodon* was known only from strata of the Ladinian-Carnian Chañares and Ischigualasto formations in Argentina (Romer, 1970; Bonaparte, 1966; Romer, 1969b; Romer and Lewis, 1973) and the Santa Maria Formation in Brazil (Huene, 1936; Romer, 1969a; Teixeira, 1982; Martinez and Forster, 1996; Abdala and Giannini, 2002) (Fig. 1). Recently however, remains of this carnivorous taxon were discovered in Africa. Abdala and Smith (2009) reported eight different cynodont taxa from the Upper Omingonde Formation, Waterberg Basin of Namibia (Fig. 1) including four cynodont genera which were new to the Namibian fauna: *Luangwa*, *Aleodon*, an indeterminate traversodontid and *Chiniquodon*. Kammerer *et al*. (2010) described a partial lower jaw of a new chiniquodontid species, *Chiniquodon kalanoro*, in the basal Isalo II beds, or the Makay Formation of Madagascar. With the discovery of additional fossil specimens in the Triassic Upper Omingonde Formation (Smith and Swart, 2002), Namibia's fauna now represents one of the most diverse in the record of non-mammalian cynodonts from the Middle Triassic of

Gondwana (Abdala and Smith, 2009). The record of *Chiniquodon*, a rauisuchian archosaur and the dicynodont *Stahleckeria* in the uppermost levels of the Upper Omingonde Formation were interpreted as indicative of a putative Ladinian age and thus younger than remaining Middle Triassic faunas from continental Africa (Abdala and Smith, 2009; Abdala *et al*, 2013). Therefore, the remains of *Chiniquodon* that were discovered in Namibia (Fig. 1) are the only Middle Triassic remains of this important, mainly South American, taxon thus far represented in the Middle Triassic continental Africa.

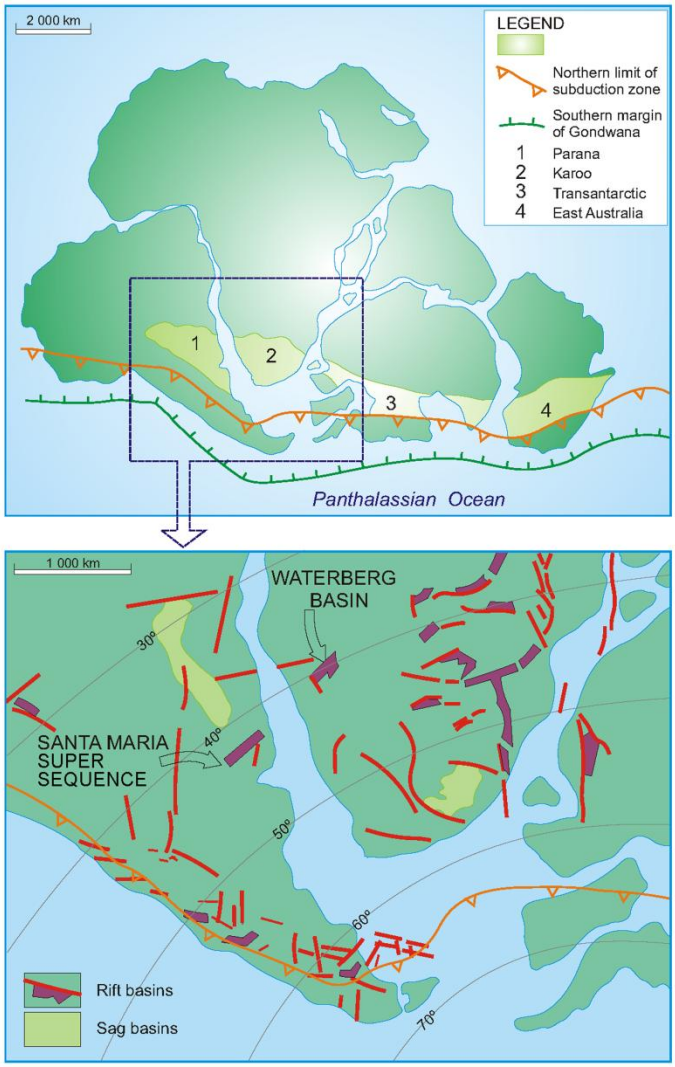

Figure 1. Triassic basins in Southern Gondwana (from Abdala *et al*, 2013).

The skull of the Namibian *Chiniquodon* was preliminarily described by Abdala and Smith (2009) and identified as *Chiniquodon* sp. The specimen is however also represented by a substantial portion of the postcranium in the collection of the Geological Survey of Namibia, which has not been described. Postcranial material for chiniquodontids from South America has been reported by various authors. Von Huene (1944) published a description of limited postcranial material of the chiniquodontid *Belesodon magnificus* (synomym of *C. theotonicus* following Abdala and Giannini, 2002) from the Santa Maria Formation of Brazil. Romer (1969a) described postcranial material of *Chiniquodon* from the Middle Triassic Santa Maria Formation of Brazil, whereas Romer and Lewis (1973) described the postcranium of *Probelesodon lewisi* (synomym of *C. theotonicus* following Abdala and Giannini, 2002) from the Chañares Formation of Argentina. Martinez and Forster (1996) reported the presence of a partial, unprepared postcranial skeleton of *Probelesodon sanjuanensis* from the Carnian Ischigualasto Formation of Argentina, which remains undescribed. Finally, Oliveira *et al*. (2009) described a partial skeleton of *Chiniquodon* cf. *theotonicus*, collected from the Therapsid Cenozone, from the Middle Triassic Santa Maria Formation, southern Brazil.

1.2. Geological settings of chiniquodontid fossil localities in South America and Namibia

The geological and sedimentological features of the formations in which chiniquodontid fossils have been collected are summarized below.

1.2.1. Chañares Formation, Argentina

The Chañares Formation was deposited during the Triassic in the northwest-southeast trending Ischigualasto-Villa Unión Basin, which forms a half-graben rift basin in western Argentina (Stipanícic and Marsicano, 2002). This formation is unconformably underlain by

the Tarjados Formation and is the lower unit of the Agua de la Peña Group, which also includes the Los Rastros, Ischigualasto and Los Colorados formations (López Gamundí *et al*., 1989; Caselli, 1998; Mancuso, 2005a, b). Rogers *et al*. (2001) and Kokogian *et al.* (2001) inferred a Ladinian age for the Chañares Formation based on fossil fauna, as well as the stratigraphic relationship with the overlying Carnian Ischigualasto Formation (Fig. 2).

The Chañares Formation is structureless, not exhibiting any laminations or cross bedding, but with an abundance of concretions and a substantial portion of volcaniclastic material (Romer and Jensen, 1966; Stipanícic, 1983; Rogers *et al*., 2001). Initially Romer and Jensen (1966) divided this formation into two informal units, an upper "bluish" unit and a lower "white" unit, based mostly on colour and fossil content. They recognised that their lower unit contained an abundance of tetrapod fossils, whereas the upper unit was devoid of fossils. Rogers *et al*. (2001) subdivided the formation into a lower unit containing an abundance of fluvial sandstones and siltstones, and an upper lacustrine claystone-siltstone unit with thin ash beds (Mancuso *et al.,* 2014). The ash beds are widespread and according to López Gamundí *et al*. (1989) were deposited by muddy streams. The lower fluvial facies preserves silicified root traces with scattered pebbles and locally abundant small brown carbonate concretions (Mancuso and Caselli, 2012). Within this facies two levels containing abundant large brown calcareous concretions were observed, as well as smaller, randomly distributed concretions. The lower concretion level, which is located midway inside the claystone-siltstone facies, yielded most Chañares vertebrate fossil remains (Romer and Jensen, 1966; Rogers *et al.,* 2001; Mancuso *et al.,* 2014). The upper concretion level lacks vertebrate fossils, although some of the concretions exhibit vertical burrows, and the layer is associated with a white tuff layer. However, few vertebrate fossils were observed inside the tuffaceous clay–siltstones.

According to Rogers *et al*. (2001) and Mancuso (2005a) the tuffaceous sandstones were deposited by river channels, whereas the claystone-siltstone facies was deposited on alluvial floodplains. The uppermost facies consists of laterally persistent, light grey and pale olive claystones and siltstones, with 'popcorn' weathering and numerous, randomly distributed sub-vertical invertebrate burrows, 10–12 cm long and 0.8 cm wide, assigned to the ichnogenus *Taenidium* (Rogers *et al.,* 2001). This facies was deposited in a shallow lake environment (Rogers *et al*., 2001; Mancuso, 2005a).

Paleosol data collected for the Chañares Formation suggests a mean annual precipitation of 250-1500 mm, representing an arid to semi-arid seasonal climate (Curtin, 2001; Gyllenhaal, 1990; Shipman, 2004).

1.2.2. Ischigualasto Formation, Argentina

The Ischigualasto Formation was deposited during the Late Carnian to Early Norian (Martínez *et al*., 2011) in the Ischigualasto-Villa Unión Basin, which is a continental extensional or a rift basin in north-western Argentina (Alcober, 1996; Currie *et al*., 2009). The lower two thirds of the formation have yielded a great diversity of fossils, including cynodonts (Martínez and Forster, 1996; Martínez *et al*., 1996, 2013; Abdala and Giannini, 2002), archosaurs (Rogers *et al*., 1993; Bonaparte, 1982, 1997; Langer, 2005), and flora (Spalletti *et al*., 1999).

The Ischigualasto Formation consists of about 300–700 m of fluvial channel sandstones, conglomerates, overbank mudstones, paleosols, and basalts from volcanic flows, all of which were deposited during the last stage of synrift tectonics (Milana and Alcober, 1994; Alcober, 1996). The thickness as well as the lithological character of the Ischigualasto Formation change laterally across the basin from the east to the west. In the east, the formation thins from 413 m to 397 m and is dominated by overbank mudstones, whereas in

the west, it thickens to 691 m and is dominated by fluvial channel sandstones. Currie e*t al*. (2009) have subdivided the Ischigualasto Formation into four lithostratigraphic members. The basal La Peña Member, comprises about 35-50 m of tan/gray sandstone and conglomerate and green/gray smectitic mudstone. The smectitic mudstone represents floodplain sediments and the sandstones represent crevasse splays. The Cancha de Bochas Member consists of about 65–125 m of mudstone and sandstone, with rare interbeddings of bentonite and basalt. Red, green, and red/gray-mottled mudstones that commonly contain abundant calcareous nodules, rhizoliths, slickensides, peds, and cutans dominate within this member. Sandstones represent fluvial channel deposits laterally associated with fine-grained sandstone and siltstone crevasse splay and levee deposits. Fine grained sanidine and plagioclase crystals were found in several thin, (< 15 cm) bentonite beds, interpreted as altered volcanic ash beds. In the east of the study area flow basalts ranging in thickness from 1 to 25 m, with vesicular to amygdaloidal textures contain plagioclase phenocrysts. The Valle de la Luna Member comprises a 250-470 m package of mudstone and sandstone, and is dominated in some areas by structureless smectitic fine-grained floodplain deposits of a dark gray colour and by channel sandstone, crevasse splay and levee deposits in other parts of the deposit. Many abandoned channel deposits in this member contain abundant carbonaceous mudstone and plant fossils. The Quebrada de la Sal Member consists of mudstone and sandstone deposits of 35–65 m thickness. The channel sandstones display four types of channel-bodies. Abundant crevasse splay, crevasse channel, and levee deposits were noted in the member. Mudstones are often pedogenically altered. A number of <15 cm thin gray and red coloured bentonite or siliceous siltstone beds were interpreted as representing altered volcanic ash deposits, which contain very-fine grained, euhedral sanidine and plagioclase crystals.

Paleosols of the Ischigualasto Formation support an increase in annual precipitation from 760 mm or less in the lower half of the formation to 760-2100 mm in the upper half of the formation and reveal dry and wet seasonal climatic extremes (Shipman, 2004).

Sanidine crystals from a tuff layer ~80 m above the base of the formation were dated at 227.8 8 ± 0.3 Ma using Argon isotopes (Rogers *et al*., 1993) and recalibrated to 231.4 ± 0.3 Ma by Martínez *et al*. (2011), whereas Shipman (2004) dated plagioclase crystals collected ~70 m from the top of the formation at 217.0 ± 1.7 Ma. In addition, Odin and Letolle (1982) dated basalts from the Alto Fault, which are correlated with basalts from the lower parts of the formation (Currie *et al*., 2009) at 229 ± 5 Ma.. These dates give the formation a Carnian-Norian age based on the latest IUGS timescale (IUGS, v 2014/02; Cohen *et al*., 2013, updated).

1.2.3. Santa Maria Formation, Brazil

Triassic deposits in Brazil are confined to the southernmost part of the Chaco–Paraná Basin and comprise the Sanga do Cabral (Early Triassic) and the Santa Maria (Middle to Late Triassic) supersequences (Zerfass *et al*., 2003). Zerfass *et al.* (2003) divided the Santa Maria Supersequence, which was deposited during the Ladinian-Rhaetic interval in the Rio Grande do Sul State, into three depositional sequences called, from young to old, Santa Maria 1, 2, and 3. The chiniquodontid specimens were collected in the basal portion of the Santa Maria Sequence 1 (Oliveira *et al*., 2009), which is up to 50 m in thickness (Zerfass *et al*., 2003). According to Machado (2004), and Rubert and Schultz, (2004) the Santa Maria Sequence 1 is composed of massive or finely laminated reddish mudstones and some carbonatic concretionary levels, corresponding to floodplain facies. Zerfass *et al*. (2003; 2004) interpreted the Santa Maria Sequence 1 as composed of a lower fluvial part, composed of massive orthoconglomerate, conglomeratic sandstone and massive to fine-grained sandstone

and siltstone deposits, indicative of low-sinuosity rivers. This is followed by an upper transgressive shallow lacustrine part, comprising massive or laminated red mudstones, indicative of shallow lake deposits. The latter deposits preserved abundant fossil vertebrate remains (Barberena, 1977; Scherer *et al*., 1995; Schultz *et al*., 2000) in association with plant material (Ianuzzi and Schultz, 1997).

Faunal correlations of this unit with the Chañares Formation suggest a Ladinian age for the base of Santa Maria Sequence 1 (Schultz *et al*., 2000; Rubert and Schultz, 2004; Abdala *et al*., 2009; Abdala and Ribeiro, 2010) (Fig. 2). Although previous biostratigraphic studies (Keyser, 1973a, 1973b; Pickford, 1995; Lucas, 1998; Holzförster *et al*., 1999) suggest that the deposition of the Santa Maria Supersequence and the Triassic strata of the Waterberg Basin were not synchronous, Zerfass *et al*. (2003) assume that the Santa Maria Supersequence and the Triassic deposits, the Omingonde Formation of the Waterberg Basin are roughly coeval.

Martin (1961) and Zerfass *et al*. (2003) suggest that the Santa Maria Supersequence represent the remains of a rift basin and might have been controlled by the same fault system, which controlled the deposition of Triassic and Jurassic sediments in the Waterberg Basin of Namibia, the Omaruru–Waterberg Fault Zone.

Petrographic evidence suggests climatic seasonality during the deposition of the Ladinian Santa Maria Sequence 1 and a more humid phase within an overall semiarid climate, but this increase in humidity was not enough to keep perennial water bodies (Zerfass *et al.,* 2003).

1.2.4. Isalo II Beds/ Makay Formation, Madagascar

The Morondava Basin of Madagascar is the largest of three basins, the other two being the Majunga and Diego basins, bordering the Mozambique Channel (Boast and Nairn,

1982). The Morondava Basin is approximately 1000 km long and is situated on the west coast of Madagascar (Boast and Nairn, 1982). Active Faults during "Karoo" times formed horsts and grabens, which trend 20° NW or 20º NE (Boast and Nairn, 1982). The basin was infilled with 11 km of nonmarine "Karoo" sediments, succeeded by a thinner post-Karoo sequence of marine and non-marine beds (Boast and Nairn, 1982).

Three groups known as the Sakoa, Sakamena, and Isalo Groups represent the infilled sediments (Boast and Nairn, 1982). Terrestrial beds of the Isalo Group have been correlated to the Karoo and most of it has been interpreted as Jurassic (Boast and Nairn, 1982). This group is 5000 to 6000 m thick in the Morondava Basin and has conventionally been divided into Isalo I, Isalo II, and Isalo III beds (Besairie, 1953). The beds comprise fine-grained, ochre coloured sandstones with lenses of variegated shales (Besairie, 1953; Boast and Nairn, 1982).

A chiniquodontid specimen, UA 10607, represented by a partial mandible, was collected in the ‘basal Isalo II’ beds, also known as the Makay Formation (Langer *et al*., 2000); near Antanandava in the southern Morondava Basin. According to Kammerer *et al*. (2010) *Chiniquodon kalanoro* and other fossils collected in the ‘basal Isalo II’ beds/ Makay Formation; provide conflicting biostratigraphic signals, making an age assignment to the fauna difficult (Kammerer *et al*., 2010). However, the ‘basal Isalo II’ fauna is most similar to the Santa Cruz do Sul fauna of the Ladinian Santa Maria Formation of Brazil (Kammerer *et al*., 2010). Thus the best-supported age assessment for the ‘basal Isalo II’ beds, based on the cynodont record, is a Ladinian age assignment (Kammerer e*t al*., 2010). Specimens were collected in a sequence of variegated, bioturbated red and green clays and siltstones, and gray cross-bedded fine- to coarse-grained sandstone deposits (Kammerer *at al*., 2010).

1.2.5. Upper Omingonde Formation, Namibia

Several authors have reported the accumulation of Triassic-Jurassic megasequence deposits in north-western Namibia in the southwest-northeast trending, elongated Waterberg-Erongo depository (Reuning and Huene, 1925; Gevers, 1936; Porada *et al*., 1996). Smith and Swart (2002) reported that the Triassic Omingonde Formation was deposited in the rift Waterberg Basin, next to an active fault margin, the northeast-southwest trending Waterberg-Omaruru Fault Zone, with tectonism controlling sediment accumulation.

Holzförster *et al.* (1999), sub-divide the Omingonde Formation into four units, each composed of sets of related depositional cycles separated by erosional or sediment bypass contacts, with the two upper units corresponding to the Upper Omingonde Formation. Since this study focuses on the Upper Omingonde Formation, only the last two upper units will be considered. Holzförster *et al.* (1999) interpret the unit three, represented by a thickness of 220 m, as confined channel deposits. Within this unit, there are twelve upward fining depositional cycles of 8 to 30 metres having two main facies: a) a laterally amalgamated gravelly arkosic channel facies and b) a pale purple sandy mudstone facies. Deposition occurred within confined channels of a mixed-load dominated river system during deposition of the first facies, as well-developed upward-fining units are associated with sandstones having narrow channel widths. Paleo-current directions indicate high channel sinuosity, characteristic of meandering rivers.

A floodplain environment is reflected for the second facies, with crevasse splays providing thin lenticular sandy intercalations in areas distal to the main active channels. The palaeosols preserved in unit three are few and fairly immature, suggesting a rather arid environment with relatively low groundwater tables. Deposits of unit four are interpreted as floodplain dominated with a total thickness of 100 metres. It can be subdivided into 22 depositional cycles with a variable thickness of 1.5 to 13 m, represented by three main facies:

a) an isolated single channel facies, b) a laminated fine sandstone facies and c) a bioturbated mudstone facies. The first facies indicates a network of shallow, interlacing, poorly confined channels which are well-developed in distal braid-plains. Such environments are particularly common in arid regions. The second facies represents an upper flow regime deposition and waning stages of sheet flood events. The third facies implies a floodplain environment with shallow ephemeral lakes existing during wet seasons, whereas dry periods favoured desiccation and pedogenic modification. According to Holzförster *et al.* (1999) and Wanke (2000) a progressive change in environmental and climatic conditions occurred during deposition of the Upper Omingonde Formation, where a braided river system in a semi-arid climate changed to a more meandering river system with decreasing discharge rates in a wetter environment.

Smith and Swart (2002) also propose switching from a single, wide, shallow braided system to a narrow series of meander belts separated by floodplains but they indicate that the change of depositional environments happened over a short time period of five million years. These authors recognized three sedimentological facies associations within the Upper Omingonde Formation: 1) loessic plains with saline lakes and ponds, 2) gravel bed meandering rivers on semi-arid floodplains and 3) sand bed meandering streams on semi-arid loessic plains with saline ponds. Several fossils were discovered in loessic mudrocks of the formation.

The exact origin and stratigraphic position of the fossils collected by Holzförster *et al.* (1999) and Keyser (1973a, b) are difficult to establish. Abdala and Smith (2009) proposed that most fossils collected by Holzförster *et al.* (1999) came from their units representing the Middle Omingonde Formation and the base of the Upper Omingonde Formation. They also noted that Holzförster *et al.* (1999) misinterpreted the stratigraphic position of the *Erythrosuchus* skeleton (re-identified as a rauisuchian by Abdala and Smith, 2009) as coming

from their unit one, which is equivalent to the Lower Omingonde Formation. The original in situ position of the rauisuchian would have been in the Upper Omingonde Formation (Abdala and Smith, 2009). According to Abdala and Smith (2009) the stratigraphic position of Keyser's three arenacous horizons and the fossils he collected in relation to these, are not well defined either and the stratigraphic schemes used by Smith and Swart (2002), and Holzförster *et al.* (1999) do not match with Keyser's (1973a, b). Initially the Omingonde Formation, was interpreted as having an Olenekian-Anisian age (Keyser, 1973a, b; 1978; Kitching, 1995). However, in recent years the top levels of the Upper Omingonde Formation have been interpreted as Ladinian, based on faunal records of *Chiniquodon*, a rauisuchian archosaur and the dicynodont *Stahleckeria* (Abdala and Smith, 2009) (Fig. 2).

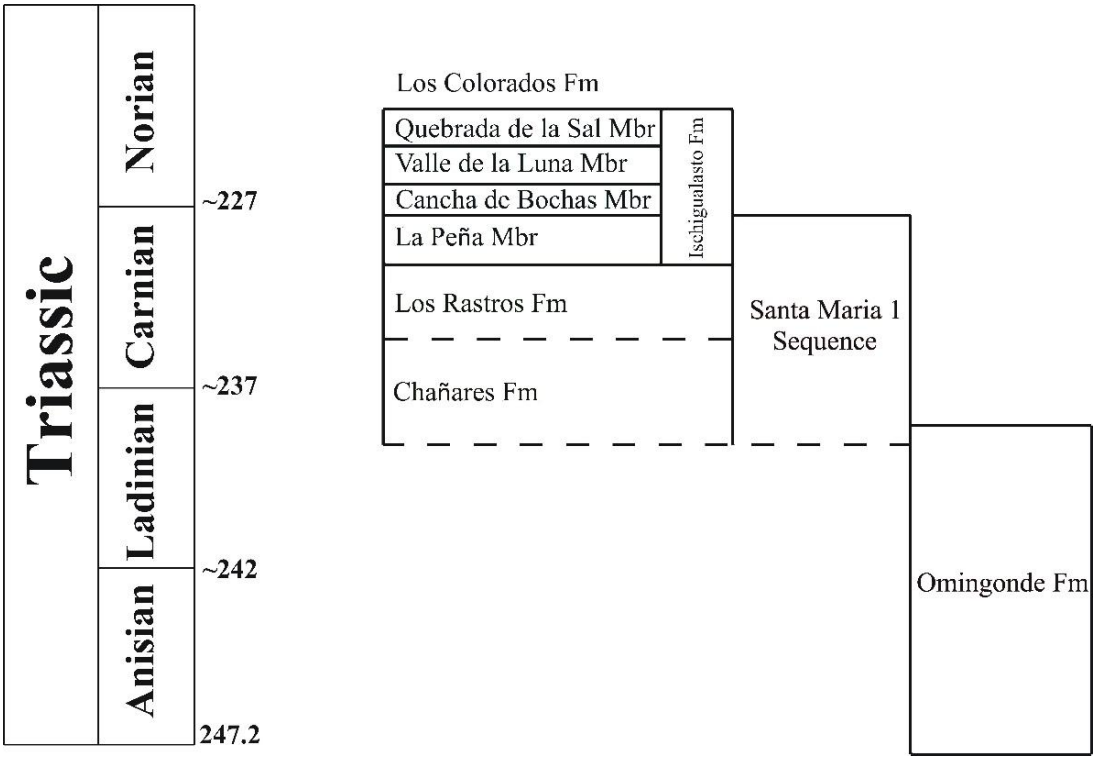

Figure 2. Stratigraphy of chiniquodontid fossil bearing geological units in South America and Namibia.

2. Chapter Two

2.1. Objectives and Hypotheses

There is a general lack of research on the postcranium of cynodonts (and therapsids in general), which resulted in its knowledge being well behind in relation to cranial information (Rubidge, 2013). At the same time it is not common to find postcranial material associated with the skull, especially in medium-to-large animals as is the case of the Namibian *Chiniquodon*. The main focus of this research will be to provide a full description of the postcranial material that has been found associated with the *Chiniquodon* skull from the Upper Omingonde Formation and to compare it to the postcranial material of the same genus from Argentina and Brazil. The research will also involve a comparison of the skull of the Namibian *Chiniquodon*, to previously described chiniquodontids from South America, in order to make a definite taxonomic identification of the fossil.

It is interesting to highlight that the upper faunal cluster from the Upper Omingonde Formation is most similar to faunas from Brazil, Argentina, Tanzania and Zambia (Abdala and Smith, 2009) than with that of South Africa. Surprisingly there is no similarity of this faunal cluster with the nearby fauna from the Burgersdorp Formation of the South African Karoo Basin. Are these differences related to age, or are these perhaps influenced by paleo-environment and palaeo-climate, and ultimately by Middle Triassic geography?

Differences and/or similarities in palaeo-climate and palaeo-environment during Triassic times in South America and Namibia, which can be gained from the analysis of geological sections and their interpretation, may provide insights into the Middle Triassic vertebrate faunas from Africa and South America, assumed to be roughly contemporaneous with that of the Upper Omingonde Formation. This will be investigated through literature review as well as architectural element analysis of geological sections measured in the

Waterberg and Omaruru River areas, and petrographic analysis of rock samples taken from the geological sections.

The following hypotheses were investigated.

1. Based on the recently defined diagnostic cranial characters for the Family Chiniquodontidae, is the specimen found in the Upper Omingonde Formation of Namibia (GSN F315) a member of the family?
2. Based on cranial and postcranial information, is GSN F315 member of the same species as the South American and Madagascar *Chiniquodon*?
3. In which palaeo-environmental and palaeo-climatic conditions did chiniquodontids live in Namibia during the Middle Triassic?

Institutional abbreviations. ESI, Evolutionary Studies Institute, University of the Witwatersrand, Johannesburg; MCZ, Museum for Comparative Zoology, Harvard University, Cambridge, Massachusetts; GPIT, Institut und Museum für Paläontologie der Universität Tübingen; GSN, Geological Survey of Namibia (National Earth Science Museum); PVL, Colleción Paleontología de Vertebrados Lillo, Universidad Nacional de Tucumán, Argentina; UFRGS PV-T, Universidade Federal do Rio Grande do Sul, Paleontologia de Vertebrados-Triássico, Porto Alegre, Rio Grande do Sul, Brasil.

3. Chapter Three

3.1. Material and methods

GSN OM-3 (field number) consists of catalogued material GSN F315, collected by Dr Roger Smith in 1995, housed at the National Earth Science Museum at the Geological Survey of Namibia (Fig. 3). The material comprises a complete skull with mandibles, the axis, five cervical ribs, two thoracic vertebrae, ten thoracic ribs, five lumbar vertebrae and four associated ribs, five sacral vertebrae and ribs, seven caudal vertebrae and ribs, partial right and left scapular blades, partial procoracoids and coracoids, partial right clavicle, complete left clavicle, partial right manus, right and left pelvises, right and left femora, tibia and right fibula and partial right pes. The Namibian material was mechanically prepared by Thilivhali Nemavhundi at the ESI, University of the Witwatersrand, Johannesburg.

Comparative material studied includes MCZ 3616, MCZ 3781, MCZ 4002, MCZ 4164, GPIT 40, PVL 3820, UFRGS PV-0146-T, UFRGS PV-1051-T, NMQR 809, NMQR 3542, TM 83, OUMNH TSK 34, USNM 22812, and BP/1/1730.

Analysis of palaeo-environmental and depositional settings of rock and fossil assemblages during the Triassic of Namibia and South America was done through a literature review, as well as field section descriptions and petrographic analysis of samples from the Upper Omingonde Formation. As the full spectrum of environments is generally best developed in the Waterberg area (Holzförster *et al*, 1999) a good geological section representative of the Upper Omingonde Formation was located on Farm Okawaka, then measured and sampled. A second section was measured and described on Farm Omingonde where the specimen under study was originally collected. Six outcrop samples were collected based on the identification of different litho-facies and architectural elements. Rock colors

were recorded in dry conditions. A Brunton Compass was used to measure paleocurrent data from cross lamination structures in various lithological beds.

Figure 3. Specimen GSN F315-1 comprising of three unprepared blocks with postcranial material of *Chiniquodon*.

Freshly cut rock samples were used to prepare standard thin sections for petrographic studies of mineralogy using an Olympus BX 35 polarising light microscope. Identification of architectural elements was done following Miall's architectural element analysis (1977, 1985, 2000).

4. Chapter Four

4.1. Results

4.1.1. Systematic palaeontology

Order THERAPSIDA Broom, 1905

Infraorder CYNODONTIA Owen, 1861

Family CHINIQUODONTIDAE von Huene, 1936

Genus CHINIQUODON von Huene, 1936

Chiniquodon sp. nov.

Locality. Next to the banks of the Omaruru River within red, nodular siltstone of the Upper Omingonde Formation on Farm Omingonde 96, Otjiozondjupa Region, central Namibia (S 21˚ 03’ 43” E 16˚ 23’ 15”).

Diagnosis. The new, unnamed taxon is a medium sized chiniquodontid (basal skull length: 19.1 cm) with seven postcanines. The specimen from Namibia was identified as *Chiniquodon* based on several features in the skull, which it shares with *C. thotonicus* from South America including a low arched zygoma, sectorial postcanines without serrations; and an elevated sagittal crest is in relation to the skull profile (Abdala and Giannini, 2002; Fig. 4). Postcranial features that differentiate the Namibian *Chiniquodon* specimen from other chiniquodontids are: lumbar and sacral vertebral spines are more robust and orientated more posteriorly; thoracic ribs have a strong proximal curvature following the head; distal articular surfaces of the sacral ribs are triangular or spoon-shaped (also observed in one specimen from Brazil); in lateral view, the procoracoid is less rounded than that of other chiniquodontids with a large ellipsoid procoracoid foramen; the angle between the proximal and distal ends of the clavicle, is more gently curved at ~145˚; the unguals of the manus are not as strongly developed; the neck of the ilium is robust; the angulation between the edge of the posterior lamina and the

margin of the neck is large at ~90˚; and the ischium has a large ellipsoid obturator foramen and is more than twice the size of the pubic plate.

Comments. In relation to the skull length, the snout makes up 45 per cent, orbits 18 per cent and temporal region 37 percent. These proportions are close to those reported by Abdala & Giannini (2002: fig.7) for the South American *Chiniquodon* specimens. However, these values should be considered with caution because of deformation in the skull of the Namibian specimen. The curvature in the clavicle might have been affected by post mortem deformation.

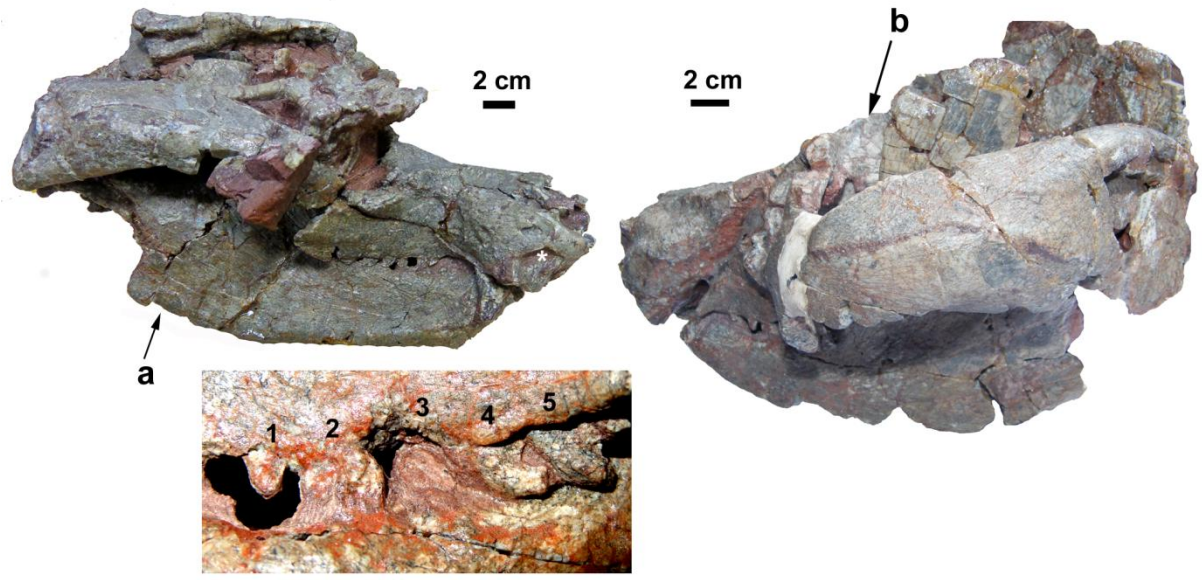

Figure 4. *Chiniquodon* skull in left and right lateral views and detail of the left postcanine series below (see sectorial teeth with strong re-curvature, length of the tooth series is 3.9 mm). **a** indicates the posterior curvature of the dentary; **b** indicates elevated saggital crest; ***** indicates the step between incisors and canines. Basal skull length 19.1 cm.

4.2. Description of postcranium

The surface of the bones is cracked with several post-mortem fractures including evidence of dorso-ventral compression of some elements. The lumbar, sacral and caudal

elements are articulated and the sacral vertebrae are preserved in articulation with the right and left pelvis, which preserve the ilium, pubis and ischium in articulation. The left humerus is in natural position with the head located in the glenoid cavity. The right hind limb, including the pes is almost completely preserved and positioned on top of the skull. The left scapula is articulated with a nearly complete procoracoid, whereas the right scapula shows the acromion process very close to the medial margin of the clavicle in a position probably close to natural. Thoracic ribs are mostly without articulation with vertebrae and several are fossilized adjacent to each other.

4.2.1. Axial Skeleton

4.2.1.1. Vertebrae

Twenty vertebrae are preserved and include the axis, two thoracic, five lumbar, five sacral and seven proximal caudal vertebrae (Fig. 5, Table 1). The axis is preserved, slightly out of place, against the occiput of the skull next to the occipital condyle. It is seen laterally with an anteroposteriorly oriented neural spine, which is wide dorsally. The posterior portion of the spine forms a pointed protrusion. The prezygapophysis is not visible, but the facet for the atlas arch is present next to the occipital condyle. The centrum is elongated and the odontoid process barely projects anteriorly beyond the anterior end of the centrum (Fig. 5).

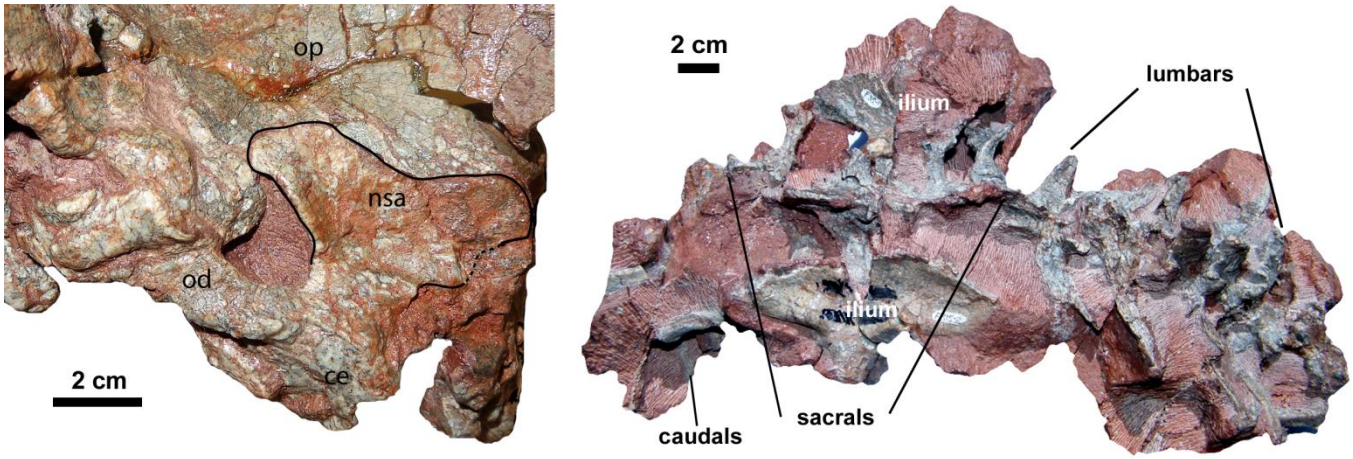

Figure 5. Lateral view of axis (left) and dorsal view of lumbar, sacral and caudal vertebrae series (right). Abbreviations: nsa, neural spine axis; ce, centrum; op, occiput; od, odontoid process.

The first vertebra in the block that includes lumbar and sacral elements is the last thoracic vertebra. The centrum of this thoracic is longer than wide and is almost cylindrical. There are thickened rims on the anterior and posterior edges, with the bone flaring out more at the anterior than the posterior edge in lateral view. Most of the posterior thoracic vertebra are still covered in matrix, except for a small portion which shows the transverse process, which is nearly articulated with the tuberculum of a thoracic rib. A third loose thoracic centrum is poorly preserved and is almost cylindrical in shape.

Five articulated lumbar vertebrae are present, with only two of them having a complete neural spine. The spines are robust at the base, becoming thinner towards the apex, are slightly posteriorly oriented (Fig. 6) and the tip is ellipsoid in cross section.

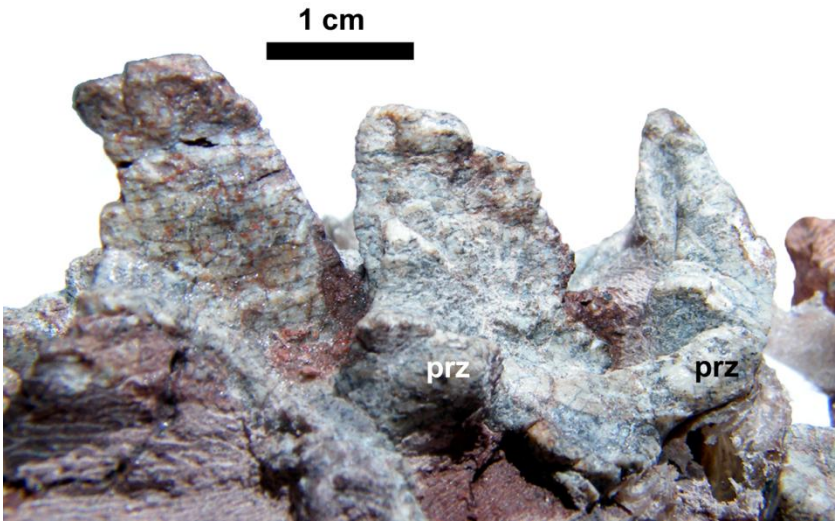

Figure 6. Lateral view of neural spines of the lumbar vertebrae. Abbreviations: prz, pre-zygapophysis.

The lumbar centrum is longer than wide, has a cylindrical morphology and displays thickening in the anterior and posterior edges. The pre-zygapophysis of the posterior lumbars is vertically oriented (Fig. 6).

Five sacral vertebrae were preserved in succession (Fig. 7). Three neural spines are visible of which two are just as tall and robust as the lumbars, and directed posteriorly. The sacral spines do not thin out as much towards their apexes, as the lumbar spines. The zygapophyses are much less robust in the sacral than the lumbar vertebrae and continue to reduce in size posteriorly towards the caudals. The three anterior centrae of the sacral vertebrae are longer than wide, and are almost cylindrical. They present thickened ventral rims anteriorly and posteriorly.

Seven proximal caudal vertebrae are preserved. They progressively become smaller posteriorly and are much smaller than the lumbar and sacral vertebrae. The zygapophyseal facets are vertical or slightly oblique (Fig. 8). The spines of the preserved caudals have all

been broken off, but their cross section indicates that they were much less robust than those of the vertebrae of the lumbars and sacrals.

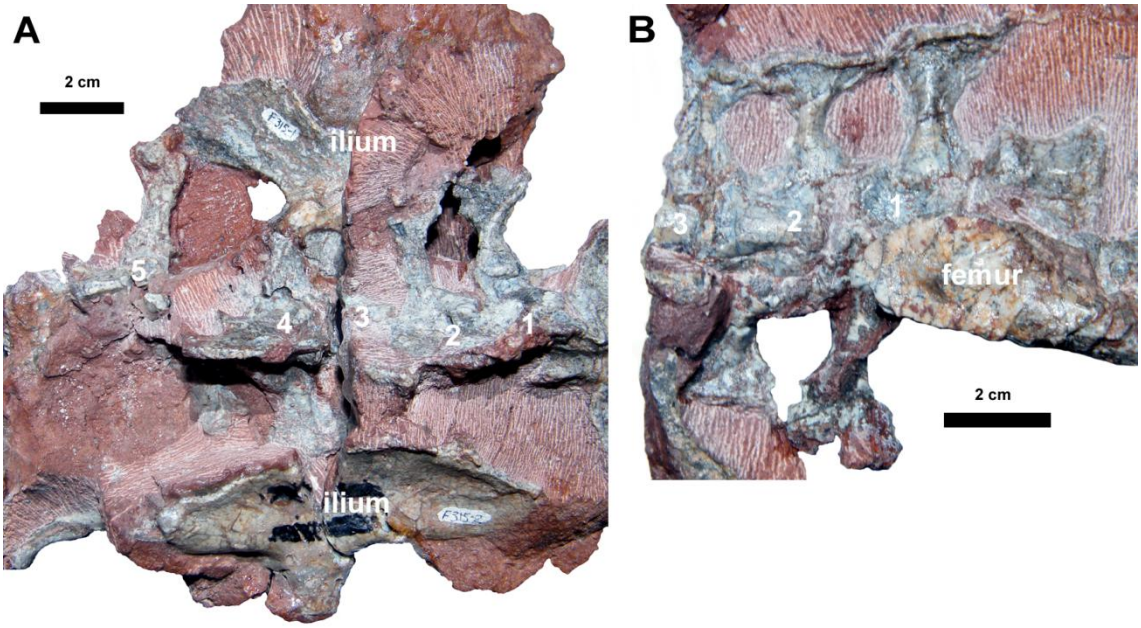

Figure 7. A, sacral series in dorsal view; B, first sacrals in ventral view. Numbers identify sacral elements.

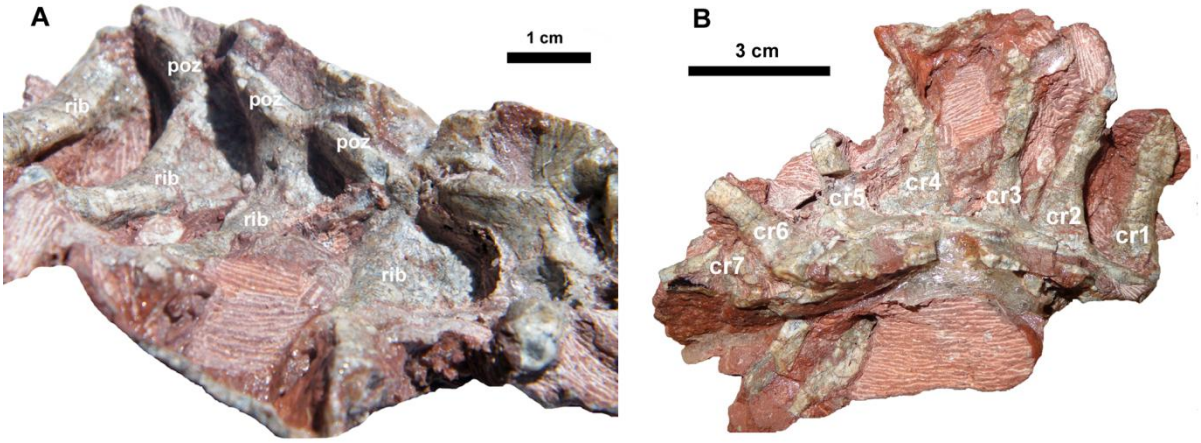

Figure 8. A, dorso-lateral view of caudal vertebrae, showing the broken neural spines, and anterior and posterior zygapophyses; B, dorsal view of proximal caudal ribs. Abbreviations: poz, prostzygapophysis; cr, caudal rib.

Table 1. Vertebrae measurements.

Vertebrae Measurements (cm)			
Bone Element	**Height**	**Length**	**Width**
Last lumbar centrum anterior posterior		1.93	1.29 2.13 1.56
Lumbar spine	2.18		
First sacral vertebra centrum		1.71	1.38
Second sacral vertebra centrum		1.81	1.49

4.2.1.2. Ribs

None of the ribs bear costal plates. The ribs are articulated to the vertebral elements in the lumbar, sacral and caudal vertebrae, whereas thoracic and cervical vertebrae are isolated.

4.2.1.2.1. Cervical Ribs

Three of the five cervical ribs preserve the proximal part of the rib, which has a flattened triangular shape with one side flaring outward slightly. In two of the cervical ribs a thin elevated ridge is seen running from the proximal end of the rib in the middle of the triangle toward the distal broken end (Fig. 9).

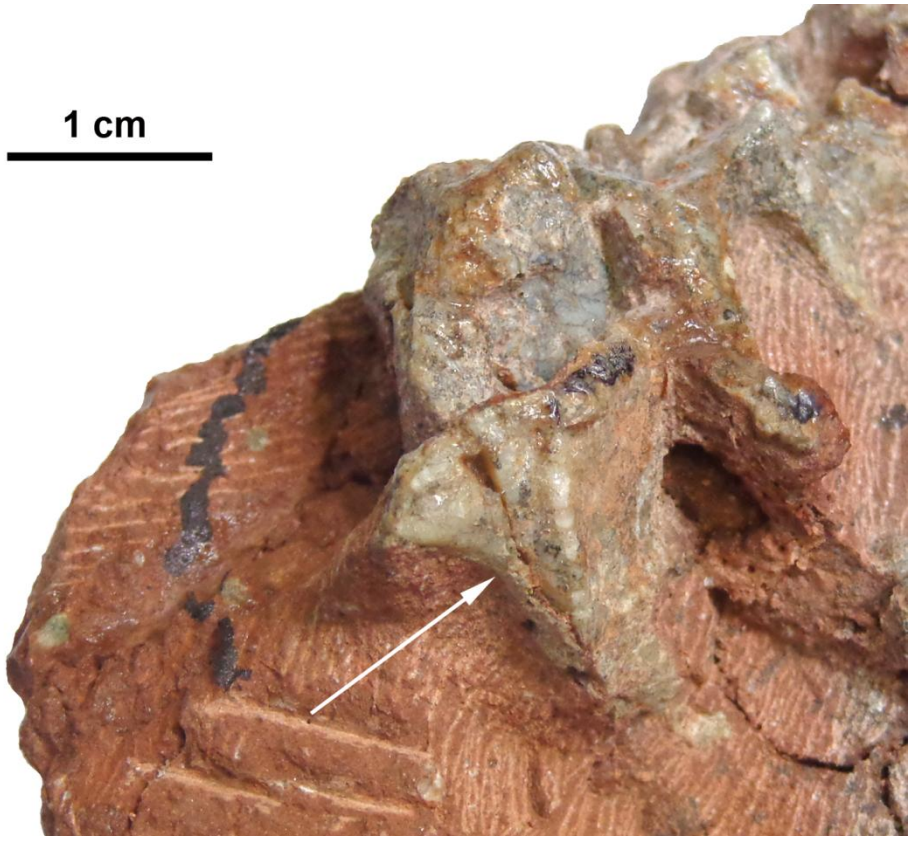

Figure 9. Cervical rib in posterio-lateral view with thin elevated ridge.

4.2.1.2.2. Thoracic Ribs

Several slender thoracic ribs have been preserved. Two anterior ribs preserve a very pronounced proximal curvature with the tuberculum being ellipsoid in cross section. These ribs show the same degree of proximal curvature, suggesting that this condition is not due to deformation. The capitulum in both ribs has been broken off, but as expected, would have formed a y-shaped morphology with the tuberculum. Ventrally, five of the ribs show a ridge (Fig. 10) on the anterior aspect of the shaft and a shortened capitular process is visible in one of the ribs. The most posterior thoracic rib, which nearly articulates with the transverse process of the second last thoracic vertebra, preserves both the tuberculum and capitulum. The facets of the tuberculum and capitulum merge to form a continuous curved facet, giving

the most anterior end an almost flattened triangular shape. A clear ridge on the anterior aspect of the shaft is preserved.

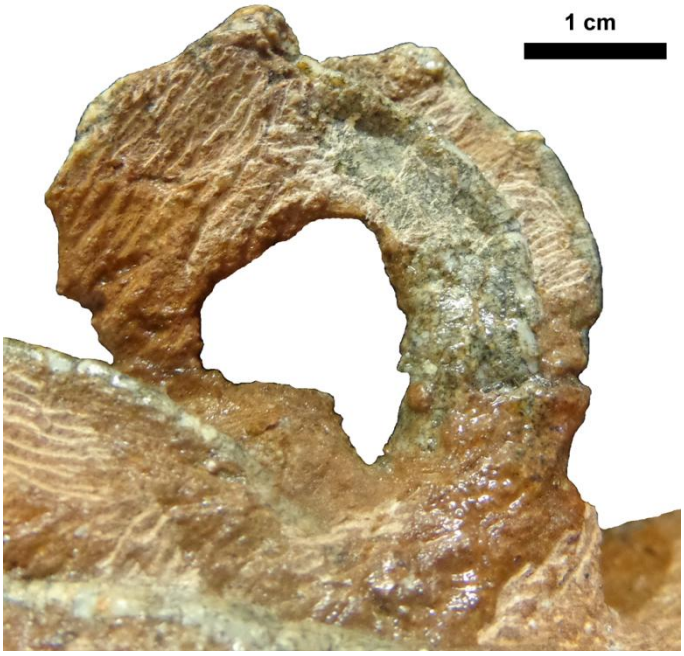

Figure 10. Thoracic ribs in lateral view with pronounced proximal curvature and thin elevated ridge.

4.2.1.2.3. Lumbar Ribs

Four lumbar ribs are preserved (Fig. 5). The first pair of visible lumbar ribs is disarticulated from the transverse processes of the vertebrae, and the last three pairs are fused to the transverse process. All the preserved ribs are directed anteriorly.

The proximal ends of the lumbar ribs are broad where they attach to the transverse processes and each rib thins out laterally and dorso-ventrally towards the distal end. In cross section the ribs are dorso-ventrally flattened and each rib has a very slight anteriorly directed twist.

4.2.1.2.4. Sacral Ribs

There are five sacral ribs fused to the transverse processes of the vertebrae (Fig. 7, Table 2). The first three ribs are broad proximally, tapering into a thin, short shaft and ending in a slightly wider proximal end (which appears as a shallow spoon in some of the preserved ribs). These ribs are quite straight, have a short shaft, and connect to each other distally. In dorsal view the fourth right sacral rib has a much wider distal end compared to the proximal end. This rib has a slight curve with the distal end directed more anteriorly. The shaft is not clearly visible and may have been affected by compression. The proximal portion of the fifth left rib has a concave area just above the outward projected line of contact between the rib and vertebra. The rib twists slightly towards its distal end and has a pronounced rounded projection directed posteriorly. This projection may be the result of preservation. The fifth rib articulates with the edge of the posterior lamina of the left ilium. The first three right sacral ribs show a general reduction in size posteriorly, whereas the fifth left sacral rib does not follow the trend and is slightly longer than the other ribs.

4.2.1.2.5. Caudal Ribs

Seven caudal ribs are fused to the transverse processes of their corresponding vertebrae, which have been dislocated from the original position. These ribs are broad at their proximal ends and thin slightly toward the distal end. The caudal ribs also display a slight curvature with a convexity directed anteriorly.

Table 2. Sacral rib measurements.

Rib Measurements (cm)		
Bone Element	**Length**	**Width**
First right sacral rib	2.40	
Proximal end		1.21
Shaft		0.73
Distal end		1.67
First left sacral rib	2.93	
Proximal end		1.06
Shaft		0.65
Distal end		1.90
Second right sacral rib	2.05	
Proximal end		1.15
Shaft		0.41
Distal end		1.60
Second left sacral rib	2.03	
Third right sacral rib	1.90	
Proximal end		1.15
Shaft		0.31
Distal end		1.26
Fourth right sacral rib	3.01	
Proximal end		1.20
Shaft		0.70
Distal end		1.97
Fifth left sacral rib	4.01	
Proximal end		1.17
Shaft		0.64
Distal end		1.47

4.2.1.3. Pectoral Girdle and Forelimb

4.2.1.3.1. Scapula and Procoracoid

A partial right scapular blade is preserved with the proximal portion (ventral to the acromion process) and distal lamina being lost (Fig. 11 A, Table 3). Anterior to the scapula is an extremely thin bone interpreted as the dorsal most portion of the scapular blade. The overall shape of the blade is very slender and tall, and cranial and caudal borders show a

gentle lateral flexure. The greatest surface area is in the most distal portion of the blade. The supracoracoid fossa deepens towards the proximal, lateral area of the blade, but is shallow distally. The anterior and posterior margins of the blade have elevated ridges, which gradually diminish toward the distal portion of the blade. The elevated ridges and the deep supracoracoid fossa give the blade a deeply concave morphology (Fig. 11 A).

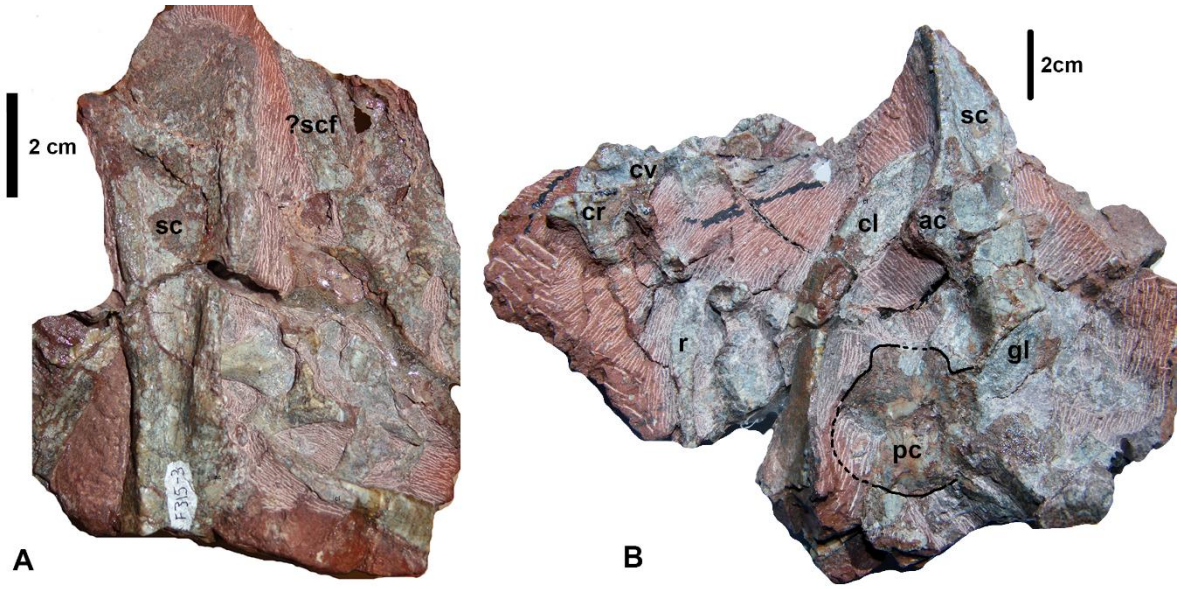

Figure 11. A, lateral view of right scapula; B, lateral view of left proximal scapula, glenoid, procoracoid and clavicle. Abbreviations: sc, scapula; ?scf, scapular fragment; ac, acromion process; cl, clavicle; pc, procoracoid; gl, glenoid; cv, cervical vertebra; cr, cervical rib; r, rib.

The left scapular blade lacks the distal portion (Fig. 11 B, Table 3). The acromion process is large and wide at its base, where it is positioned well above the neck of the scapula. It protrudes outward.

The partially preserved left procoracoid is rounded antero-laterally (Fig. 11 B, Table 3). The procoracoid foramen is large, ellipsoid and directed laterally.

4.2.1.3.2. Clavicle

Only a portion of the proximal end of the right clavicle is preserved, whereas almost the complete left clavicle is present (Fig. 11 B). The proximal end of the clavicle is gently concave for the reception of the acromial process. The clavicle curves at an angle of ~145˚ between its proximal and distal ends and flares outward distally (Fig. 12). The length of the clavicle is approximately 8.29 cm excluding the proximal tip, which is covered in matrix below the scapula (Table 3).

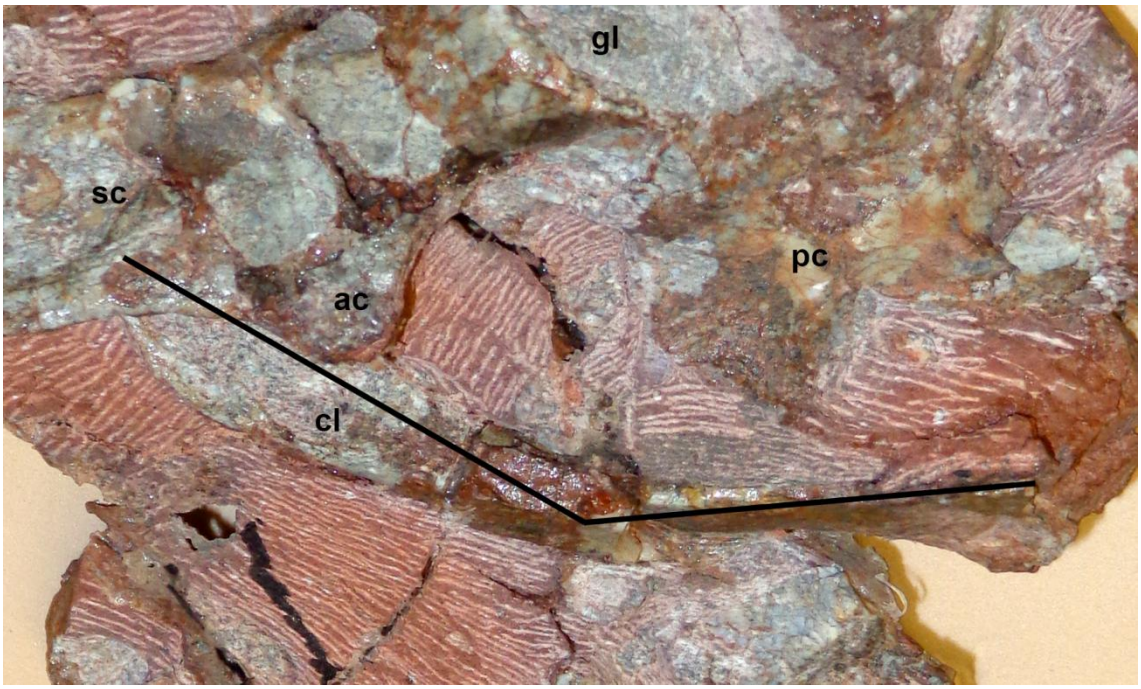

Figure 12. Left clavicle (length 8.29 cm) in dorso-lateral view. Abbreviations: cl, clavicle; sc, scapula; ac, acromion process; pc, procoracoid; gl, glenoid. Line is showing the angulation of ~145˚ between the proximal and distal portions of the bone.

Table 3. Pectoral girdle measurements.

Pectoral Girdle Measurements (cm)		
Bone Element	**Length**	**Width**
Right scapula	10.11	
Right anteroposterior proximal scapula		1.82
Right anteroposterior distal scapula		3.24
Edge of scapula to acromion process		2.40
Left scapula acromion process base		1.55
Left scapula acromion process protrusion	0.74	
Left procoracoid foramen diameter	0.91	0.66
Left clavicle excluding medial part	8.29	

4.2.1.3.3. Manus

Semi-articulated elements of the right manus (see measurements in Table 4) are preserved in plantar view (Fig. 13). Two recognizable carpals (interpreted with caution as the lateral central and the third distal); metacarpals II, III, IV, V; the first, second and third phalanges of digits II and III; and fragmentary first and second phalanges of the digit IV; are preserved. The metacarpals and phalanges in digits II and III are articulated.

The putative lateral central has a rectangular to ovoid shape with a ventral projection on the lateral side. It is situated proximal to the third distal. The third distal has an irregular shape, a notch or concavity directed antero-laterally, and a robust crest on the surface. The fifth metacarpal preserves the dorso-ventrally flattened proximal portion and the shaft. The fourth metacarpal also preserves the proximal portion and shaft. The proximal portion is wider that the shaft, but not dorso-ventrally flattened as in the fifth. Only broken fragments of the first and second phalanges of the fourth digit remain preserved. Third metacarpal is

complete and is as robust and stout as the fourth metacarpal, and wide both proximally and distally. First phalange of the third digit is much shorter and far less robust than the metacarpal. Second phalange has the same size as the first and widened proximal and distal ends, presenting an hourglass shape. Third phalange is a claw, partially preserved, with a high proximal portion which gently narrows towards the tip. Second metacarpal is complete with a wide and semi-circular distal end. First phalange is less robust than the metacarpal, but quite long. Second hourglass-shaped phalange is shorter and more robust than the first one. Claw has a high proximal end and a gentle dorsal convex curvature towards the tip, whereas the ventral surface is slightly concave.

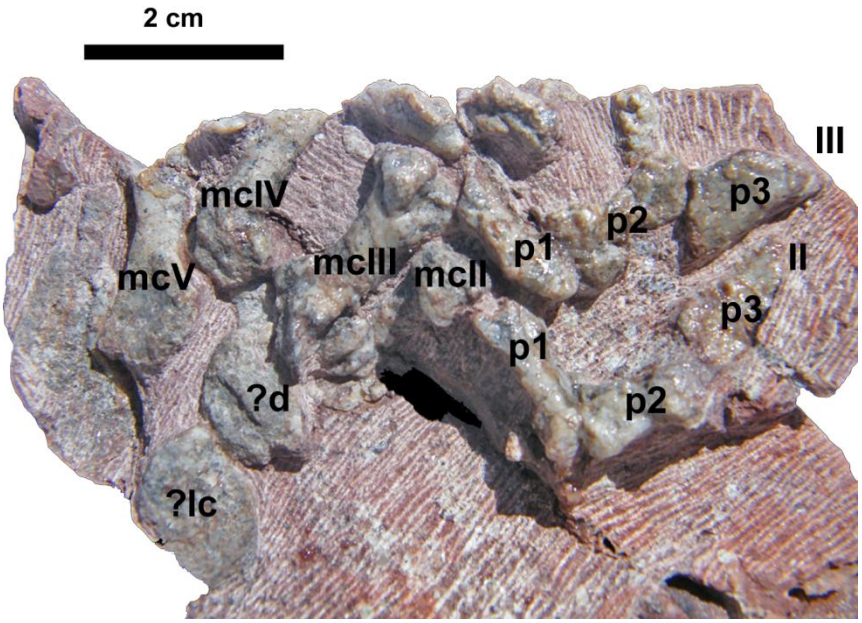

Figure 13. Plantar view of manus. Abbreviations: ?lc, lateral central; ?d, third distal; mcII, second metacarpal; mcIII, third metacarpal; mcIV, fourth metacarpal; mcV, fifth metacarpal; II, second digit; III, third digit; p, phalange.

Table 4. Manus measurements.

Right Manus Measurements (cm)		
Bone Element	**Length**	**Width**
Lateral central	0.97	1.47
Third distal	1.05	1.46
Metacarpal digit II	1.88	proximal 0.67 distal 0.85
Metacarpal digit III	2.41	proximal 1.22 distal 1.22
Metacarpal digit IV proximal end	1.99	proximal 1.09
Metacarpal digit V proximal end	2.10	proximal 1.27
Digit II first phalange	1.74	proximal 0.74 distal 0.94
Digit II second phalange	1.16	proximal 0.84 distal 0.60
Digit II third phalange	1.62	proximal base 0.84
Digit III first phalange	1.65	proximal 0.73 distal 0.78
Digit III second phalange	1.46	proximal 0.93 distal 0.65
Digit III third phalange	1.23	proximal 0.89

4.2.1.4. Pelvis and Hind Limbs

4.2.1.4.1. Pelvis

The pelvic bones are slightly disarticulated, although they remain more or less in the correct body position (Figs. 14, 15).

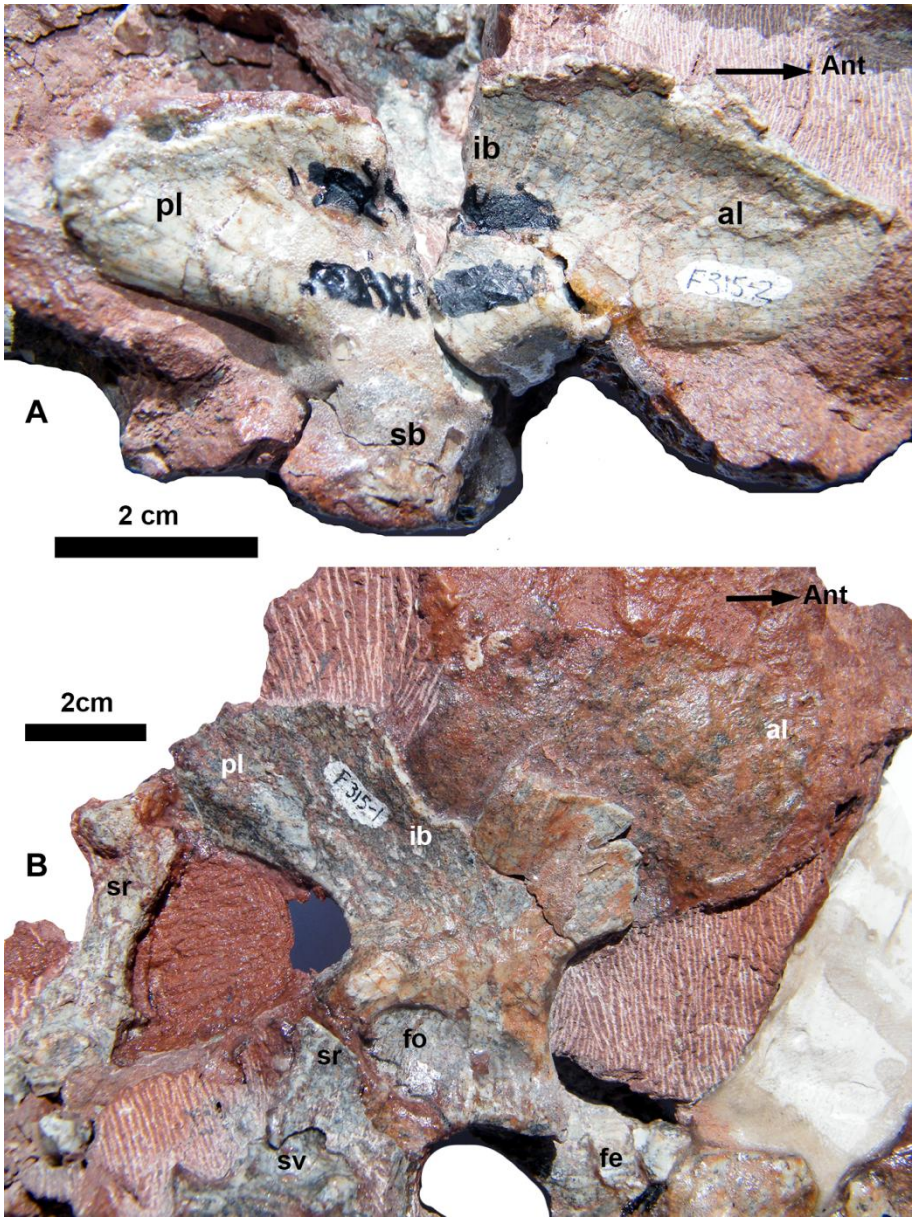

Figure 14. A Lateral view of right ilium. B Medial view of left ilium. Abbreviations: pl, posterior lamina; ib, iliac blade; al, anterior lamina; sb, supra-acetabular buttress; Ant, anterior; sr, sacral rib; sv, sacral vertebra; fo, acetabular foramen; fe, femur.

4.2.1.4.1.1. Ilium

Both ilia are preserved (Table 5). The right ilium has flipped over, so that it is visible laterally (Fig. 14 A), while the left ilium has flipped ventrally and its medial side is visible (Fig. 14 B). The anterior edge of the left ilium is broken. However, its border remained as a mould on the matrix, clearly indicating the anterior outline of the bone. Slight striations can

be seen on both the ventral and medial sides of the left ilium, but they are more conspicuous on the lateral side of the right ilium. There is also a shallow ridge running along the posterior border of the left ilium.

Each ilium is anterior-posteriorly elongated, with the anterior lamina more elongated than the posterior (Fig. 14). The angulation between the border of the posterior lamina and the posterior margin of the neck is 90˚ or slightly more. The neck is very robust. The supra-acetabular buttress of the right ilium is visible and does not project laterally. The acetabular facet is directed ventrally.

4.2.1.4.1.2. Pubis and Ischium

Left pubis and ischium are displaced dorsally in relation to those on the right side. The only connection that remains between these elements is through the posterior portion of the ischial plate, in what seems to be a sutured union (Fig. 15). Pubic plate is flat and shows a lateral concavity, and a rounded postero-distal margin. Anteriorly the right pubic plate preserves a clear facet. Dorsally the plate produces a flat projection (broken in the specimen) which is connected to the pubic neck. Ischial plate is flat and more than twice the size of the pubic plate (Table 5). Ischial tuberosity is directed postereo-ventrally and has a thin elevated margin for muscle attachment. Obturator foramen is well developed and more or less ellipsoid with the anterior margin being slightly larger than the posterior one. Pubis and ischium contribute nearly equally to the margin of the foramen.

Right acetabular notch is badly broken and only the margin of the left notch can be seen, where the ischium contributes a larger portion than the pubis.

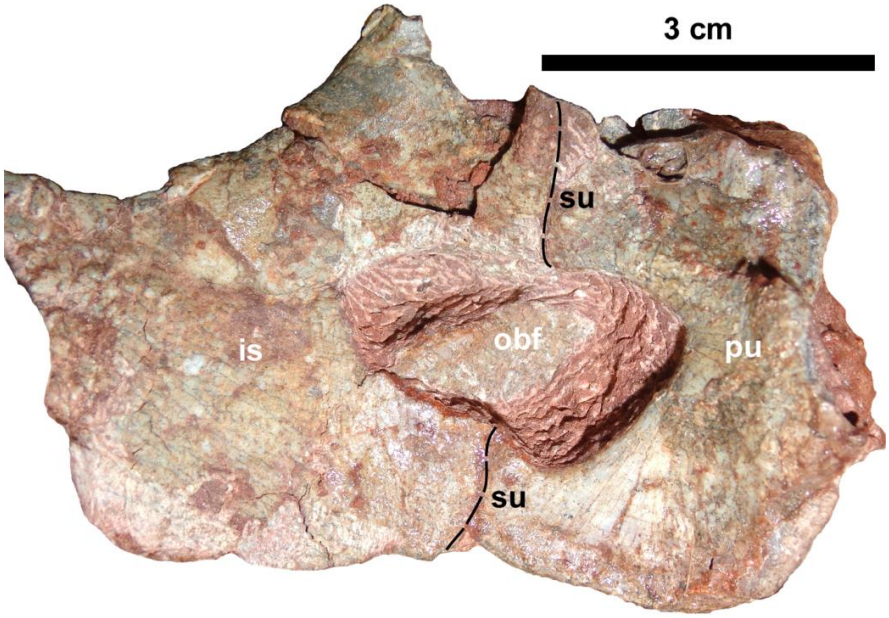

Figure 15. Right pubis and ischium in lateral view. Abbreviations: is, ischium; pu, pubis; obf, obturator foramen; su, suture.

Table 5. Pelvis measurements.

Pelvis Measurements (cm)		
Bone Element	**Length**	**Width**
Right pubis and ischium	8.76	
Left ilium	9.03	
Right ilium neck		2.70
Left ilium neck		2.70
Right obturator foramen	3.06	
Anterior margin		1.85
Posterior margin		1.65

4.2.1.4.2. Femur

The right femur is almost completely preserved, except for the proximal portion (Fig. 16) and the left femur is fully preserved (Fig. 17, Table 6). Both femora are slender and particularly short, and the shaft of the femur is thinner than the proximal and distal ends. In ventral view, the lesser trochanter is very indistinct and its distal end is not visible. The fossa

for the insertion of the adductor muscle is very shallow. The lateral and medial condyles are flattened, and the lateral condyle is almost double the size of the medial condyle.

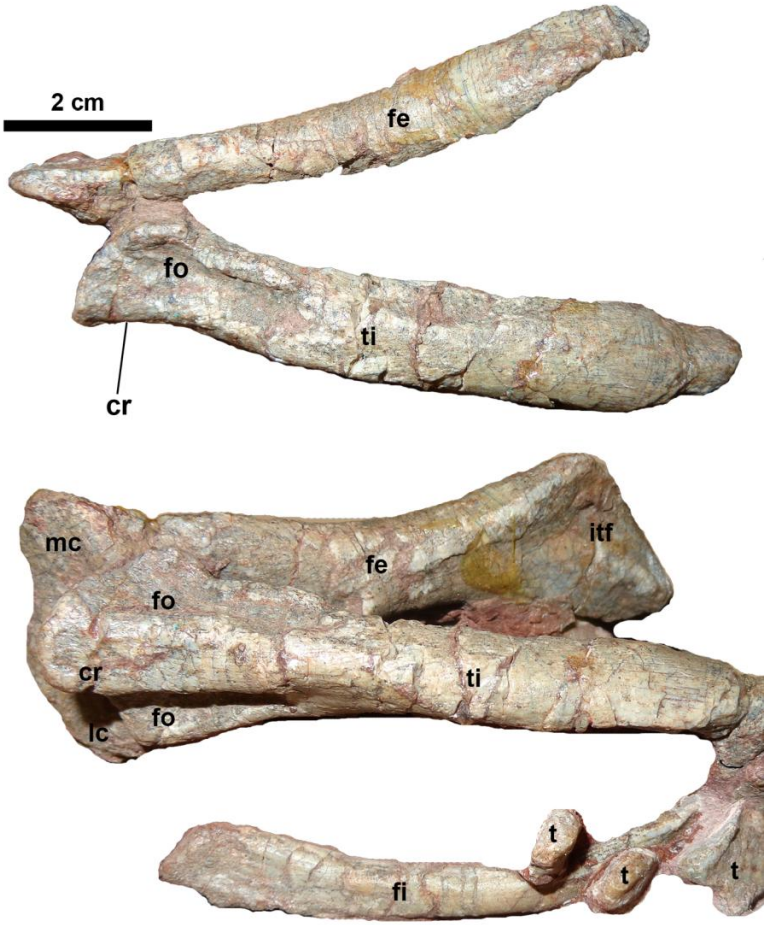

Figure 16. Right femur, tibia and fibula in lateral view above, and in ventral (femur) and anterior view (tibia), below. Abbreviations: fe, femur; ti, tibia; fo, fossa; cr, cnemial crest; mc, medial condyle; lc, lateral condyle; itf, intertrochanteric fossa; t, tarsal.

The proximal end of the left femur shows a well-developed head with a strong dorsal orientation. A large area of the head is also visible in the proximal margin of the bone (i.e., oriented towards the acetabulum). The greater trochanter is closer to the proximal end of the bone and faces laterally and somewhat dorsally. The lateral surface between the head and the trochanter is slightly concave, whereas distally, these structures are connected by a strong ridge. The intertrochanteric fossa (for the M. pubo-ischio femoralis externus) is a large, deep

circular depression, situtated posterior to the head (Fig. 17). There is a slight elevation at the level of the lesser trochanter that separates the intertrochanteric fossa from a shallow fossa for the insertion of the adductor muscle, which is located more distally. The lesser trochanter is prominenent and oriented medially. The lateral and medial condyles have been slightly affected by breaking and slight distortion. The lateral condyle protrudes more ventrally than the medial, but this may be due to damage at the distal end of the femur. There appears to be a pronounced concavity between the lateral and medial condyles, which may be due to poor preservation and the loss of bone in this area.

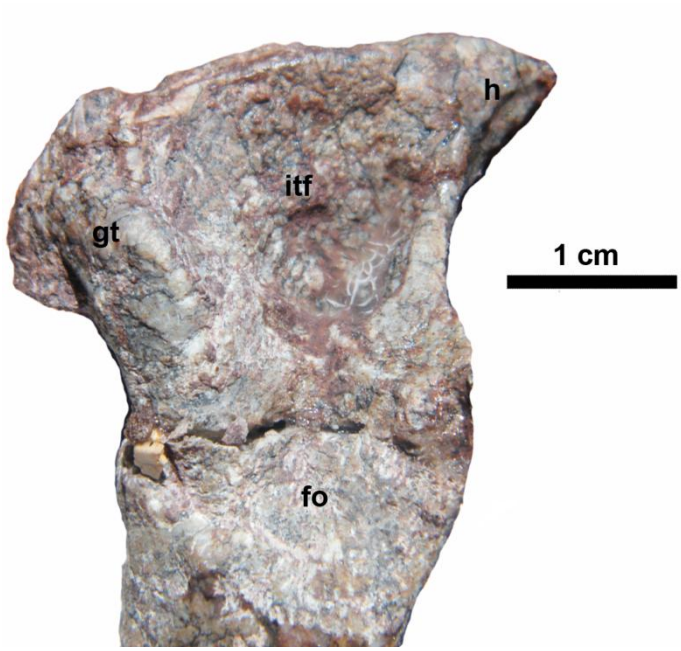

Figure 17. Proximal left femur in ventral view. Abbreviations: h, head; gt, greater trochanter; itf, intertrochanteric fossa; fo, fossa for the insertion of the adductor muscle.

4.2.1.4.3. Tibia

The right tibia is complete and articulated to the femur but, its distal end is slightly deformed (Fig. 16, Table 6). The proximal, and part of the central portion of the left tibia, is poorly preserved.

The cnemial crest is very wide proximally and its width is progressively reduced towards the middle of the shaft. Towards the lateral and medial side of the crest there are two pronounced fossae, both restricted to the proximal third of the bone (Fig. 14). These fossae cover equally sized surfaces. The shaft shows a marked crest medially which continues distally to the fossa.

4.2.1.4.4. Fibula

The right fibula is complete, but the distal portion is masked by the bones of the pes (Fig. 16, bottom, Table 6). The fibula is curved with the concavity of the curvature directed medially. The proximal margin is wider than the diaphysis and shows a shallow fossa. The fibular tubercle is reduced.

Table 6. Hind limb measurements.

Hind Limb Measurements (cm)	
Bone Element	**Length**
Left femur	12.24
Right tibia	9.41
Right fibula	10.43

4.2.1.4.5. Pes

The right pes is represented by seven tarsals and elements of four digits which are not preserved in their life position (Fig. 18).

The astragalus is visible on one side, which is assumed to be the dorsal. It shows a convexity forming an extended facet, most likely for the articulation with the tibia. Medial to this facet there is a pronounced convex belt, of which the medial margin is straight. The calcaneum is certainly the largest tarsal element, but only half of the bone is exposed and a shallow groove for the flexor tendon is evident. The visible surface is most likely the ventral

side because the ellipsoid tuber calcis is directed dorsally (i.e. in anatomical position the tuber would be directed ventrally, as is the case in other cynodonts).

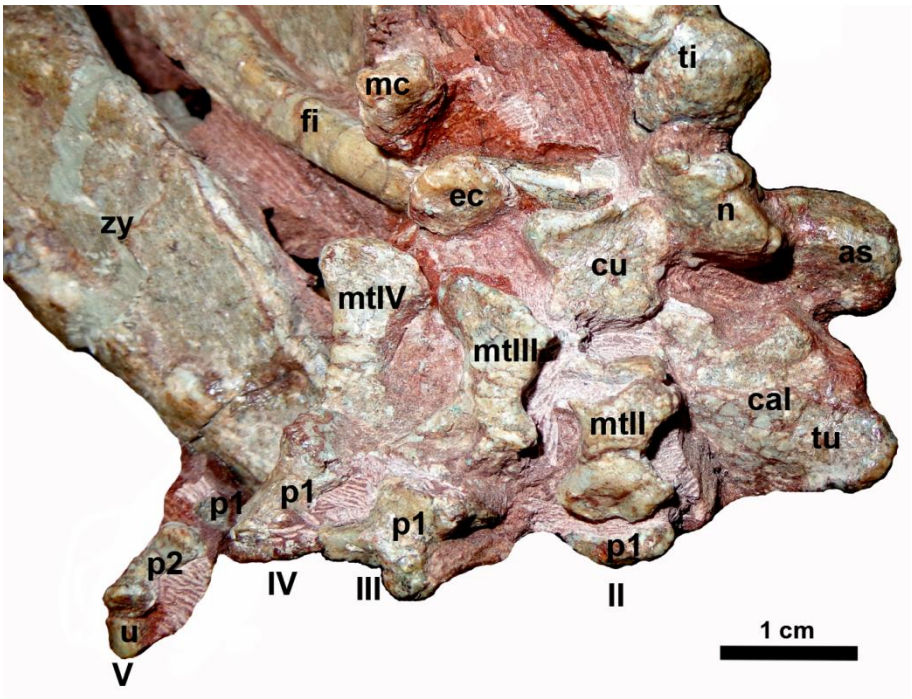

Figure 18. Dorsal view of right pes. Abbreviations: zy, zygomatic arch of skull; fi, fibula; ti, tibia; me, mesocuneiform; ec, ectocuneiform; cu, cuboid; n, navicular; as, astragalus; cal, calcaneum; tu, tuber calcis; mtII, second metatarsal; mtIII, third metatarsal; mtIV, fourth metatarsal; II, second digit; III, third digit; IV, fourth digit; V, fifth digit; p1, first phalange; p2, second phalange; u, ungual.

The navicular is a rounded element which is mostly covered by matrix and the square cuboid is positioned next to the calcaneum. The side of the cuboid that articulates with the ectocuneiform is wider than its opposite end, whereas the ventral margin has a notch. The ectocuneiform and the mesocuneiform are the smallest tarsal bones and have been displaced laterally to a position near the metatarsal IV.

Digit II has a complete metatarsal and the proximal portion of the first phalange, digit III and IV have complete metatarsals and first phalanges. An unidentified bone is preserved beneath digit IV, and is possibly another metacarpal.

Table 7. Pes measurements.

Right Pes Measurements (cm)		
Bone Element	**Length**	**Width**
Astragalus	1.69	1.58
Cuboid	1.25	1.07
Mesocuneiform	1.09	0.77
Metatarsal digit II	1.38	
Shaft		0.65
Distal end		1.18
Metatarsal digit III	1.91	
Proximal end		1.46
Shaft		0.73
Distal end		1.54
Metatarsal digit IV	1.95	
Proximal end		1.38
Shaft		0.64
Distal end		1.15
Digit III first phalange	1.14	
Proximal end		
Distal end		1.21
		1.20
Digit IV first phalange	1.52	
Proximal end		
Distal end		1.07
		0.85
Digit V second phalange	1.14	
Proximal end		
Distal end		0.73
		0.55

The metatarsals are longer and more robust than the phalanges, becoming progressively longer from digit II to IV (Table 7). Metatarsal II is robust and almost quadrangular, III is elongated and wide, and IV is slender and the longest. The proximal articulation surfaces of metatarsals III and IV are directed obliquely and dorsally. The lateral side of metatarsal III is more curved than the medial. However, the medial side of metatarsal IV is well arched, whereas the lateral side is straighter.

The proximal phalanges are shorter than the metatarsals and vary in shape from quadrangular in digit III to rectangular (i.e., longer than wider) in digit IV. Also preserved is the distal fragment of a first phalange, one complete penultimate phalange, and a partial ungual phalange articulated at the side of digit IV. These elements are interpreted as being from digit V. The penultimate element has nearly the same length as the proximal phalanges of digit II and IV, but is remarkably less robust. Only a small proximal portion of the ungual phalange is preserved and manifests a laminar structure.

4.3. Geology of the Upper Omingonde Formation

4.3.1. Farm Okawaka Section

The measured section on Farm Okawaka comprises mostly gritty conglomerates composed of rounded metamorphic lithoclasts and mudstones (Fig. 19). Two litho-facies were identified in the stratigraphic section, comprising litho-facies Gms and Fl. These were interpreted to represent two architectural elements; CH, channel deposits and OF, overbank deposits respectively (Fig. 20 A, Table 8).

Table 8. Summary of the architectural element analysis of the Okawaka section.

Architectural Element	Litho-facies	Structures, Fossil Content, Palaeocurrents	Bedding	Lateral and vertical relationships
CH 1, CH2, CH3 **Channel deposits (dipping N)**	Gritty conglomerates with rounded metamorphic lithoclasts of milky quartz, pink K-feldspar, pegmatitic granite and schist, which float in finer grit matrix of the same mineralogy (litho-facies Gms), occasionally rip-up clasts from OF	Weakly developed normal grading, with shallow cross laminations with palaeocurrent direction 30˚ NE, no fossils	Laterally pinched sheets that extend laterally for several metres, distinct occasionally erosive, undulatory, bed boundaries	The Gms litho-facies of the CH always overlies or underlies the Fl litho-facies of the OF

OF1, OF2 **Overbank deposits**	Red to green-grey-red mottled mudstone (litho-facies Fl)	Massive, contains calcareous nodules & rhizocretions, intermittent calcareous horizons, sometimes with fine parallel laminations, rarely current ripples, fossils rare	Sheet geometry, usually sharp contacts to channel deposits, occasionally deformation due to compaction	The Fl litho-facies of the OF always overlies or underlies the Gms litho-facies of the CH

Description: Architectural elements CH1, CH2 and CH3 comprise litho-facies Gms, gritty conglomerates composed of rounded metamorphic lithoclasts of milky quartz, pink K-feldspar, pegmatitic granitoids, and schist, which float in finer grit matrix of the same mineralogy (Fig. 20 B). Litho-facies Gms has weakly developed normal grading with shallow cross-laminations or bedding. Palaeocurrent measurements indicate a 30˚ north-easterly direction for the cross-laminations (Fig. 20 C). The contact to the above mudstone deposits is abrupt and undulatory. Lower bed boundaries are distinct and occasionally erosional with poorly developed channel lags containing rip-up clasts of the associated overbank deposits (Fig. 20 D). The external geometry of these channels form pinched sheets. The channel deposits can extend up to approximately 25 m laterally. The channel deposits lack fossils.

Interpretation: Architectural elements CH1, CH2 and CH3 are interpreted as channel deposits and may have been deposited during flash flood events due to their weak normal grading and coarse load. Litho-facies Gms is interpreted as debris flow deposits (Miall, 1985).

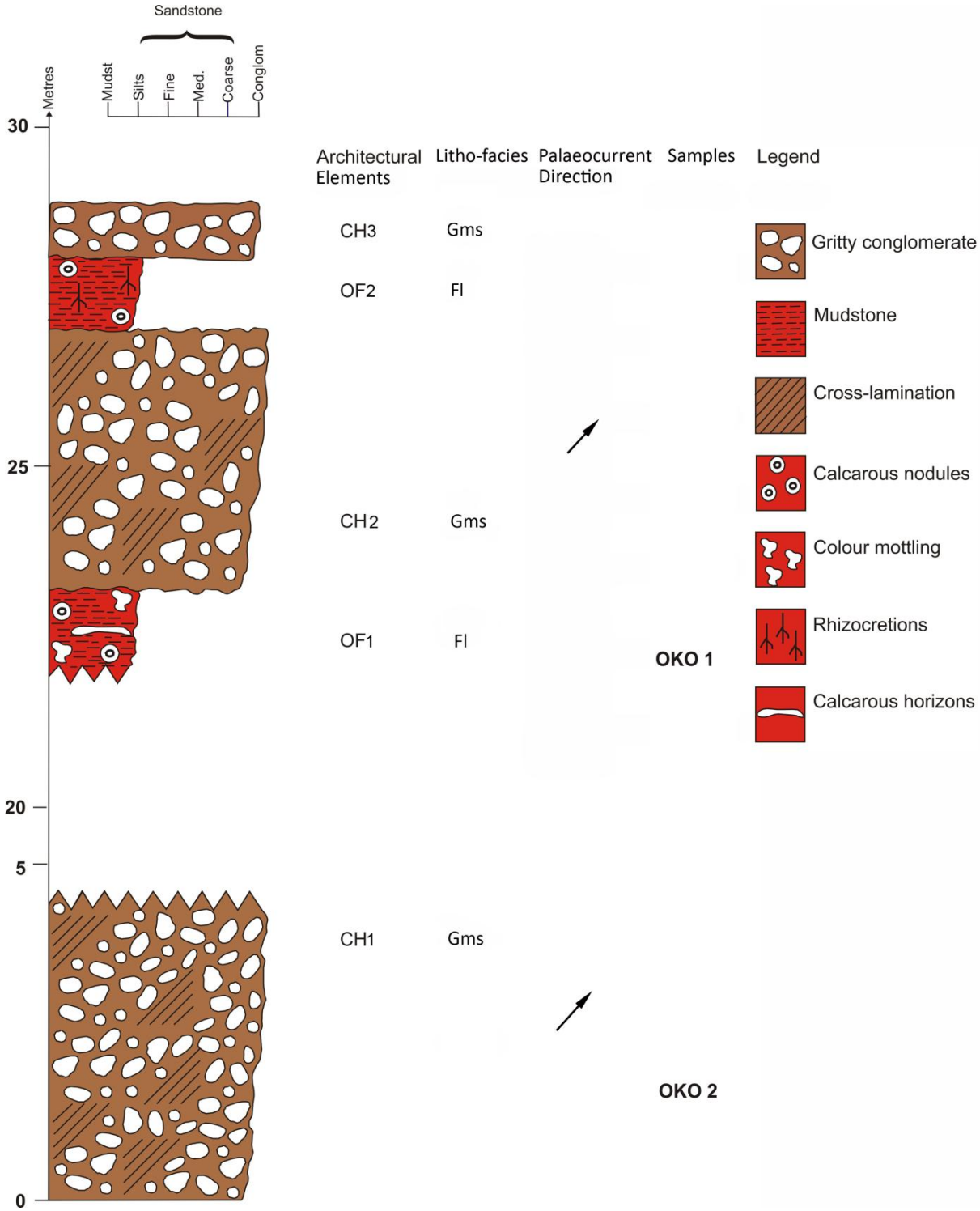

Figure 19. Log of measured section on Farm Okawaka.

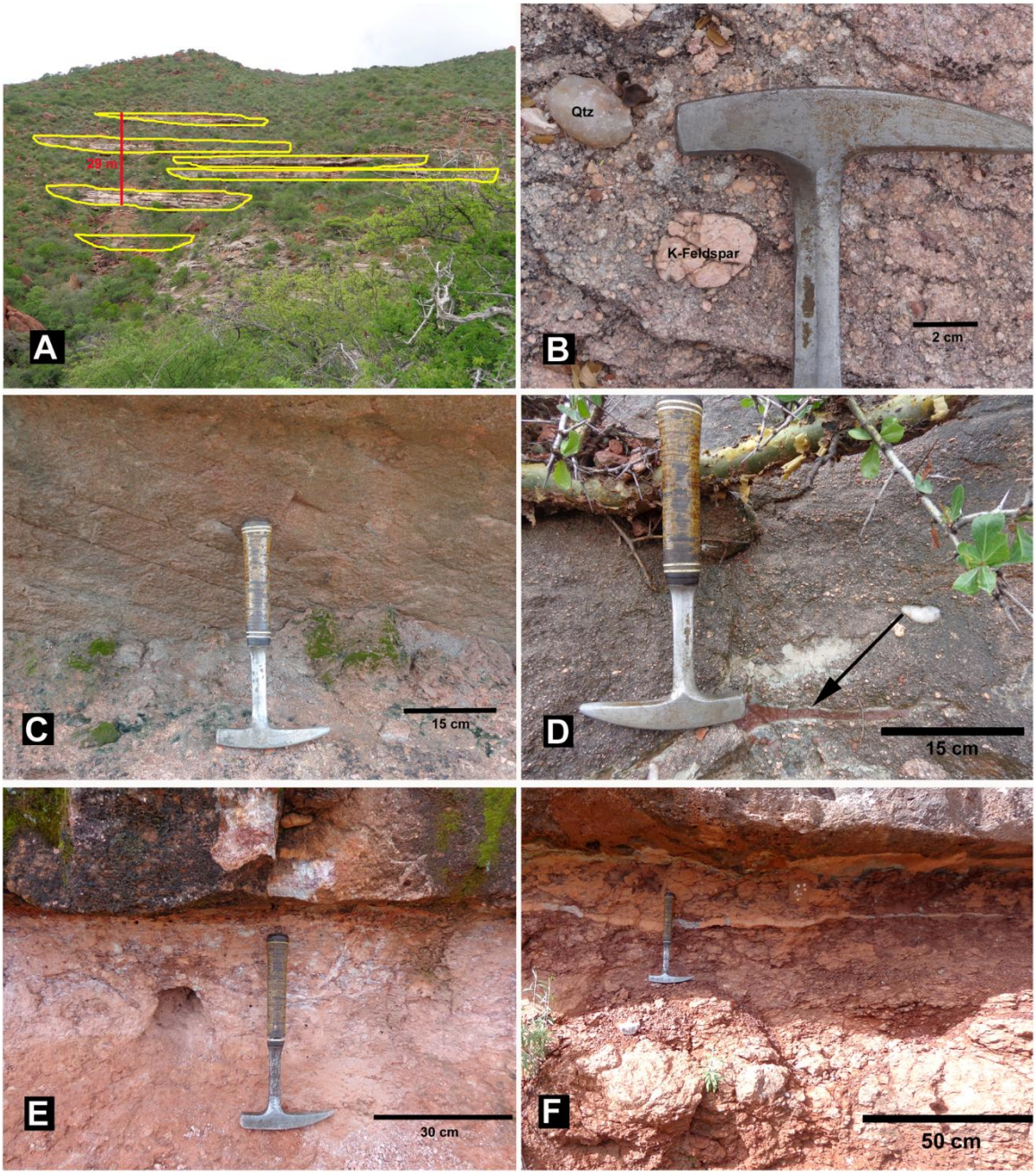

Figure 20. A, the measured section (29 m) on Farm Okawaka is indicated in red and the channel deposits are outlined in yellow; B, litho-facies Gms comprising gritty conglomerate with rounded pebbles of K-feldspar and quartz; C, architectural element CH1 with shallow cross laminations with palaeocurrent direction 30˚ NE; D, litho-facies Gms gritty conglomerate with mudstone rip-up clast from litho-facies Fl; E, litho-facies Fl with irregular grey-white calcareous nodules; F, calcareous horizon 1-5cm thick, within massive red mudstone of litho-facies Fl.

Description: Architectural elements OF1 and OF2 comprise litho-facies Fl, mudstones. Mudstones are massive and in places contain calcareous nodules (Fig. 20 E), calcareous horizons (Fig. 20 F) and calcareous rhizocretions. These mudstones often exhibit green-grey-red mottling.

Interpretation: They represent overbank deposits, which may have formed when channels spilled over and show the development of immature paleosols, which may contain fossils. Evidence for immature paleosols includes the development of greyish calcareous nodules and rhizocretions (Retallack, 2001).

4.3.1.1. Petrography of samples from Farm Okawaka

4.3.1.1.1. OKO 1

Sample OKO 1 was collected from OF1 (Fig. 21 A, Appendix 1) and shows a well sorted texture with about 60% subrounded and 40% subangular grains. The fabric is grain supported with calcite (fleshy colour) in pore spaces. Under crossed polars the following predominant mineral grains have been identified: 85% quartz (white extinction), <25 % feldspar grains, microcline (dark blue with cross-hatching), orthoclase, pyroxene (blue), and 2% micas, muscovite plates (blue extinction), as well as a few elongated biotite plates (brown extinction).

4.3.1.1.2. OKO 2

This sample was collected from CH1 and displays moderate sorting with 50% subrounded and 50% subangular grains of more than one mineral (Fig. 21 B, Appendix 1). The fabric is grain supported (95%) with a representation of the following minerals: 53% orthoclase (cracked, dark grey-blue) and microcline (blue, cross-hatched fragments), <5% calcite (creamy brown), 45 % quartz (white) and < 2% muscovite (blue-pink). Mineral grains

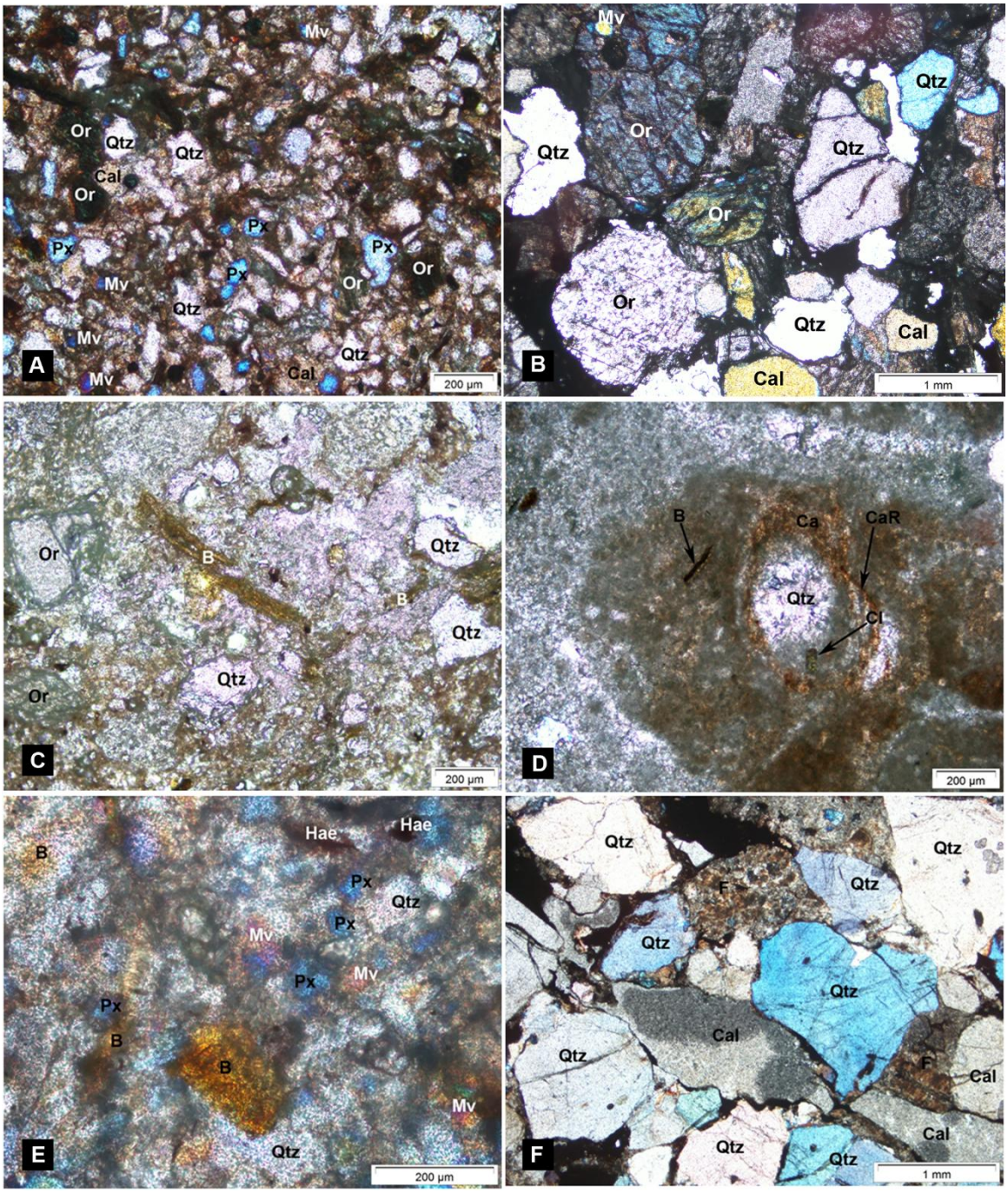

Figure 21. Micrographs of samples. A, OKO 1 from architectural element OF1 litho-facies Fl. B, OKO 2 from architectural element CH1 litho-facies Gms. C, OMI 1. D, OMI 2. E, OMI 3. F, OMI 4. Abbreviations: B, biotite; Cal, calcite; CaR, calcareous rootlet; Cl, chloritoid; F, feldspar; Hae, haematite; Mv, muscovite; Or, orthoclase; Px, pyroxene; Qtz, quartz.

vary in size from 0.5-1.5 mm with feldspars and quartz being the largest in size. Both orthoclase and microcline derive from igneous rocks. Microcline is formed when orthoclase

slowly cools and is more stable in sedimentary environments than orthoclase. Some red haematite grains were visible in the thin section as well, which may indicate some re-working of the original sediment.

4.3.2. Farm Omingonde Section

The section on Farm Omingonde comprises mostly mudstone and fine sandstone (Fig. 22). Seven litho-facies assemblages were identified in stratigraphic order, comprising litho-facies Fr, Fl, Sp, Sh, Fm, Sl, Gm and Gms. These were interpreted to represent two alternating architectural elements; CH, channel deposits and OF, overbank deposits (Table 9).

Architectural element OF is represented by three overbank deposits comprising lenses, blankets and or sheets of siltstone fines. Architectural element CH comprises four channel deposits dipping towards the south. The top part of the section is covered by at least 1m of modern sandy debris with blocks of rocks and vegetation.

Description: Architectural element OF1 comprises litho-facies Fr interbedded with litho-facies Fl, which together are 1m thick. Litho-facies Fr comprises a grey-white calcareous layer containing grey calcareous nodules and grey-white rhizocretions (Fig. 23 A). Litho-facies Fl comprises red siltstone.

Interpretation: OF1 is interpreted as the first overbank deposit. Litho-facies Fr with the calcareous layers are interpreted as palaeosols (Miall, 1985). Rhizocretions are evidence for palaeosol development (Retallack, 2001). Litho-facies Fl represents overbank and waning flood deposits (Miall, 1985).

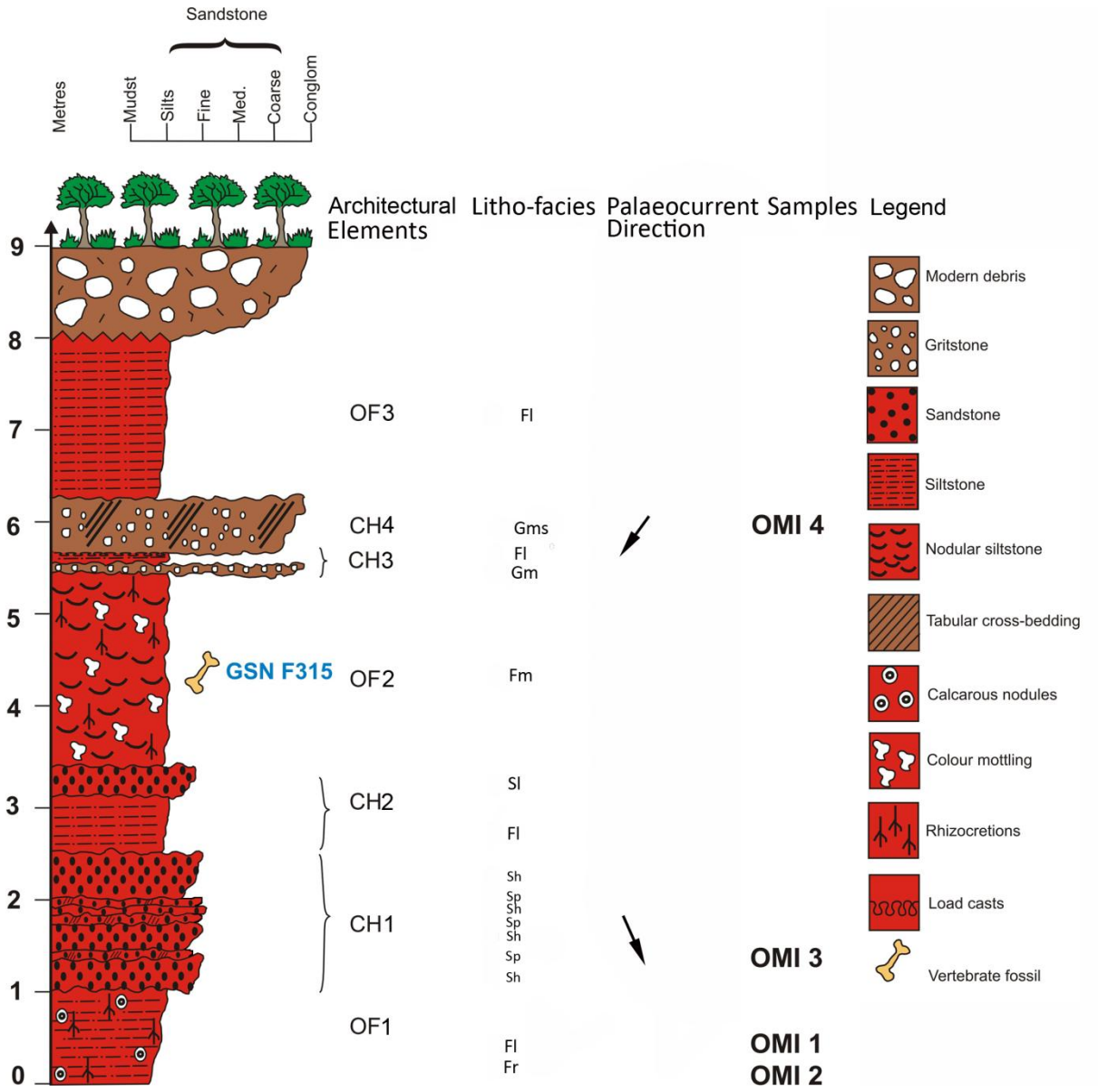

Figure 22. Log of measured section on Farm Omingonde.

Description: Architectural element CH1 comprises litho-facies Sp, which forms intercalating red-grey sandstones, and litho-facies Sh red sandstones, which together these are 1.5 m thick. Litho-facies Sp sandstones exhibit planar cross-laminations and litho-facies Sh red sandstones exhibit horizontal lamination (Fig. 23 E). Palaeocurrent measurements for the cross-laminations indicate a southerly palaeocurrent direction.

Interpretation: CH1 is interpreted as the first channel deposit. Sandstones represent channel deposits which became amalgamated (Fig. 23 D) where one channel was deposited

on top of another while mudstone was eroded away. Channel avulsion is evident from abrupt lateral termination of channels and occurrence of laterally adjacent channel deposits. Litho-facies Sp is interpreted as linguoid transverse bars and Sh is interpreted as a planar bed flow (Miall, 1985).

Description: Architectural element OF2 is 2.1m thick and comprises litho-facies Fm, siltstone fines with thick nodular, red siltstones. The nodules have a diameter range from 2-5 cm and are partially calcareous in composition. Grey-red mottling was observed in some areas (Fig. 23 B).

Interpretation: OF2 is interpreted as the second overbank deposit. The nodular development of the siltstones indicates the development of an immature palaeosols (Smith and Swart, 2002; Retallack, 2001). It was in this layer that most of the Triassic fossils, including GSN F315 were collected (Smith and Swart, 2002; Fig. 23 C; stratigraphic position of GSN F315 indicated in Fig. 22).

Description: Architectural element CH2 comprises an upward coarsening deposit of 0.9 m thickness, comprising litho-facies Fl at the bottom, represented by a red siltstone, and litho-facies Sl at the top, represented by red, fine sandstone.

Interpretation: CH2 is interpreted as the second channel deposit. Fl is interpreted as representing a waning flood and Sl may be interpreted either as a scour fill or crevasse splay (Miall, 1985).

Description: Architectural element OF3 comprises red siltstone fines of litho-facies Fl and is up to 1.7 m thick.

Interpretation: OF3 is interpreted as the third overbank deposit. However, the siltstone of litho-facies Fl contains far less calcified nodules compared to litho-facies Fm of

architectural element OF2. Litho-facies Fl is interpreted as overbank and waning flood deposits (Miall, 1985).

Description: Architectural element CH3 comprises an upward fining deposit of 0.2 m thickness, which comprises from the bottom litho-facies Gm, a layer of gravel, and at the top litho-facies Fl, a layer of red siltstone.

Interpretation: CH3 is interpreted as the third channel deposit, where litho-facies Gm and may represent a channel lag with the top litho-facies Fl representing a waning flood deposit (Miall, 1985).

Table 9. Summary of the architectural element analysis of the Omingonde section.

Architectural Element	Litho-facies	Structures, Fossil Content, Palaeocurrents	Bedding	Lateral and vertical relationships
OF1 overbank, siltstone fines	Grey-white palaeosol interbedded with red siltstone (Fl and Fr)	Massive, with calcareous nodules, calcarous, grey-white rhizocretions/rootlets	Sheet with erosive top contacts	Fl and Fr litho-facies underly the Sh litho-facies of element CH1.
CH1 channel deposit (dip S)	Intercalating fine red-grey sandstones (Sp) and red sandstone (Sh).	Intercalation of fining upward lithofacies, planar cross- laminations with southerly palaeocurrent direction, as well as horizontal laminations, no fossils	Sheet with erosive/non-erosive contacts	Sp litho-facies amalgamate vertically where mudstone was eroded away. Sp avulse laterally due to a sudden change in channel direction. Sh litho-facies form thin sheets between Sp facies.
CH2 channel	Red siltstone (Fl)	Upward coarsening, no fossils	sheets with erosive	Sl litho-facies of CH2 overlies the last Sh

deposit **(dip S)**	underlying a red fine sandstone (Sl)		contacts	litho-facies of CH1. The Sh litho-facies of element CH2 underlies the Fm litho-facies of element OF2.
OF2 overbank, siltstone fines	Nodular, red siltstone, red-grey mottling here and there (Fm)	Massive, vertebrate fossils found	sheet with erosive contacts,	Fm litho-facies overlies Sh of element CH2 and underlies litho-facies Gm of element CH3.
CH3 **channel deposit** **(dip S)**	Bottom layer of gravel (Gm) and a top layer of red siltstone (Fl)	Upward fining, massive gravel, load casts in top red siltstone;	sheet with top erosive contact to CH4 and bottom load casts contact with OF2, no fossils	Gm litho-facies overlies the OF2 Fm litho-facies. The Fl litho-facies of element CH3 undelies the Gms of element CH4.
CH4 **channel deposit** **(dip S)**	Gritstone (Gms) with angular <1.5cm pebbles	Massive, with tabular cross-bedding with palaeocurrent direction towards the SW, no fossils	sheet with erosive contacts	bottom contact with the element, CH3 litho-facies Fl, is represented by load casts
OF3 overbank, siltstone fines	Red siltstone (Fl)	Massive with calcified nodules, no fossils	blanket with erosive contacts	Fl lithofacies overlies Gms lithofacies of element CH4 and underlies modern debris layer

Description: Architectural element CH4 comprises litho-facies Gms, a gravel or gritstone layer, which is approximately 0.6 m thick. Gms contains tabular cross-bedding and angular pebbles of less than 1.5 cm size. Palaeocurrent measurements indicate a south-westerly

palaeocurrent direction. The bottom contact with litho-facies Fl (red siltstone) is marked by numerous load casts (Fig. 23 F).

Interpretation: CH4 is interpreted as the fourth channel deposit. Litho-facies Gms is interpreted as a debris flow deposit (Miall, 1985). The load casts were formed as a result of compaction after deposition, resulting in deformation of the softer sediment below by the heavier sediment above.

4.3.2.1.Petrography of samples from Farm Omingonde

4.3.2.1.1. OMI 1

Sample OMI 1 was collected from CH1 in the section. Grain size sorting is poor with the presence of 40% subangular and 60% subrounded mineral grains (Fig. 21 C, Appendix 1). Grains are matrix supported, with grains representing only 20% silty matrix and 80% mudstone. The average grain size for all mineral grains is 20-200 µm, while the average grain size for individual minerals is; quartz 10-200 µm, biotite and muscovite plates 10-500 µm, and orthoclase and other feldspars 10-200 µm. The predominant minerals are 85% quartz, less than 15% feldspars including orthoclase. The feldspars display smooth straight edges, and produce a white and grey extinction when rotating the stage. Micas make up less than 2%. Muscovite plates, with green and blue birefringence colours, and elongate-platy biotite plates with a yellowish brown birefringence colour were observed under crossed polars. Some feldspars show signs of alteration and dissolution.

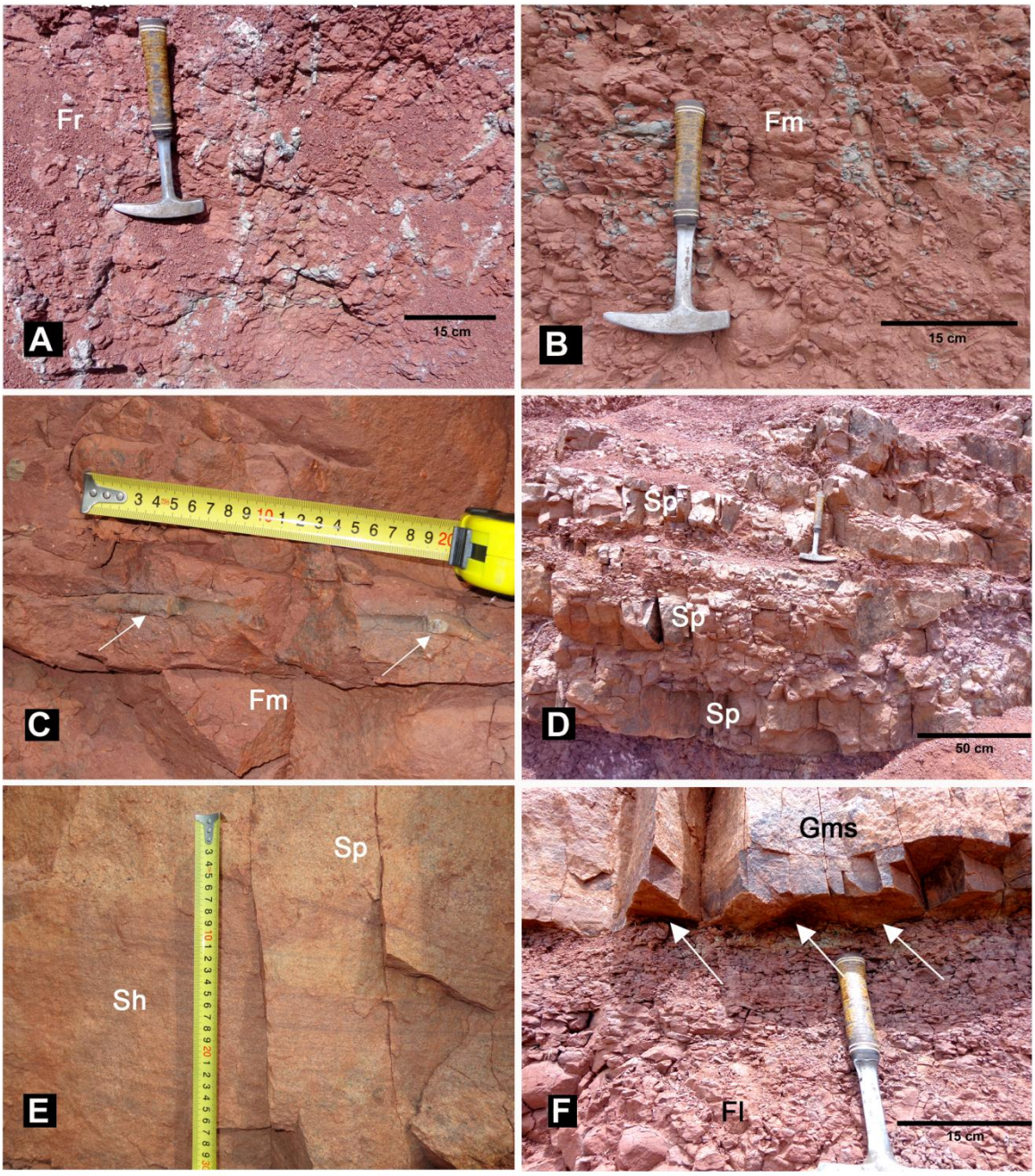

Figure 23. A, palaeosol with calcareous nodules and rhizocretions from Litho-facies Fr from architectural element OF1; B, red siltstone with mottling from litho-facies Fm from architectural element OF2; C, tetrapod rib fossil weathering out from litho-facies Fm siltstone from architectural element OF2; D, Sp litho-facies amalgamated vertically after erosion of mudstone deposits; E, architectural element CH1 comprises intercalating red-grey sandstones from litho-facies Sp, with shallow cross-laminations, and red sandstones from litho-facies Sh, with fine horizontal lamination; F, architectural element CH4 comprises litho-facies Gms, a gravel or gritstone layer (top), forming numerous load casts into the bottom contact with litho-facies Fl (red siltstone).

4.3.2.1.2. OMI 2

This sample was also collected from CH1. Grains are moderately sorted, 80% subrounded and 20% subangular. Grains are matrix supported, with grains representing 10% against 90% matrix (Fig. 21 D, Appendix 1). The micritic to calci-lutitic matrix consists predominately of calcite, which has a characteristic fleshy colour. The size of the mineral grains is much smaller than for the OMI 3 sample and grains range in size from 2-200 µm, while the average grain size for individual minerals is; quartz 2-200 µm, biotite and muscovite plates 20-200 µm, and feldspars 10-100 µm. The grains comprise 50% quartz with an undulating white grey colour extinction, 50% yellow-brown calcite, <1% feldspar grains with fractures and straight edges (grey colour), <1% elongated brown to green biotite and muscovite grains, having a typical blue and green birefringence colour scheme and black colour diffusion when the stage is turned so that the crystals are aligned for extinction.

4.3.2.1.3. OMI 3

OMI 3 was collected from OF1. This sample consists of approximately 20% subrounded and 80% subangular grains which are supported by 70% calci-lutitic matrix (Fig. 21 E, Appendix 1). The grains are smaller than those of OKO 2 sample and range in size from 20-200 µm. The average grain size for individual minerals is; quartz 50-150 µm, for biotite and muscovite 0.5-200 µm, and for pyroxene 50-100 µm. The grains consist of 80% quartz, 10% feldspar, plagioclase and pyroxene, and 10% micas (biotite and muscovite). The micas sometimes occur as plates and sometimes as elongated fibers. Traces of haematite (deep maroon-red) blebs and crystals provide evidence for alteration and re-working. The plagioclase grains show a characteristic black and white zebra stripe pattern. The quartz grains are larger than most other mineral grains and the feldspar show signs of alteration: patches and lines of black appearing at the grain edges, or even in cracks within grains.

4.3.2.1.4. OMI 4

The sample OMI 4 was taken from a sandstone from CH4. The shape of the grains includes 90% subangular and only 10% subrounded grains (Appendix 1). The fabric is 98% grain supported and grains are packed together tightly (Fig. 21 F). The matrix consists of <2% yellow-brown calcite. Mineral grains range in size from 0.5-2 mm and 90% of the grains are subangular. The average grain size for individual minerals is; quartz 0.5-1.5 mm, for muscovite plates 0.5-1.5 mm, and for feldspar and plagioclase grains 0.5-1.5 mm. The mineral grains comprise 95% quartz, 5% alakali-feldspar and plagioclase, with its characteristic zebra stripe pattern. Less than 1% muscovite has been identified by its uniaxial optical pattern when using the Bertrand Lens. Two zircon crystals were observed; these have a black edge and a blue turquoise interior. They are tiny, at the order of ~2μm. One was located inside a feldspar grain. The characteristics of this thin section are very similar to OKO 2 in terms of packing, matrix, angularity of grains and mineral content.

5. Chapter 5

5.1. Discussion

5.1.1. Postcranium

Although chiniquodontids are relatively abundant in deposits from Argentina and Brazil (Abdala and Giannini, 2002; Mancuso *et al*., 2014), the postcranium remains poorly studied, basically restricted to the contributions of Huene (1936), Romer (1969a), Romer and Lewis (1973) and, more recently, Oliveira *et al*. (2009). Three of these contributions are on material from the Brazilian Santa Maria Formation that show, overall, a very poor preservation (Fig. 24 C); Romer and Lewis's (1973) contribution on Argentinean Chañares Formation chiniquodontids is on better preserved material (Fig. 24 B), although the complete skeleton described in that contribution, MCZ 3781, is also poorly preserved (Fig. 24 A). The presence of partial, unprepared postcranial material of *Probelesodon sanjuanensis* (Martinez and Forster, 1996) was also referred, but remains undescribed.

The contribution presented in this dissertation is twofold; firstly to compare the postcranial remains of the new Namibian chiniquodontid with those of South America, and secondly to present new information on the chiniquodontid skeleton, such as the pelvis and the foot. The description of the foot of *Chiniquodon* presented is one of only a few descriptions of the foot of Triassic cynodonts.

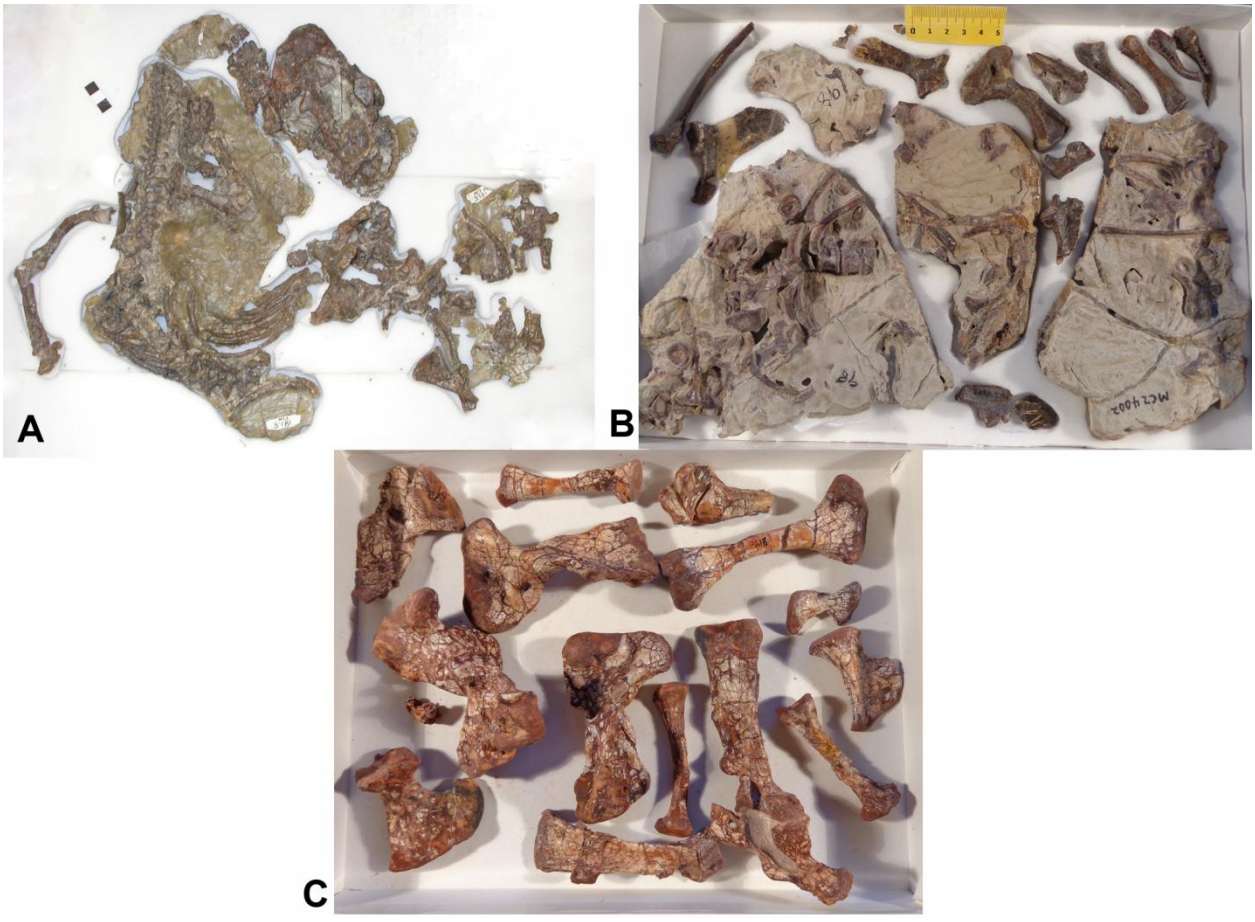

Figure 24. A, MCZ 3781 from Argentina; B, MCZ 4002 from Argentina; C, MCZ 3616 from Brazil.

5.1.1.1. Vertebrae

The pre-sacral centrae of UFRGS PV-0146-T from the Santa Maria Formation of Brazil are nearly cylindrical with thickened anterior and posterior rims (Oliveira *et al.*, 2009). The single complete thoracic centrum, a lumbar centrum and the sacral centra in GSN F315 are cylindrical longitudinally and the second-last thoracic vertebral centrum and the sacral centra display thickened bone in the anterior and posterior edges. Of the five presacral vertebrae described for GPIT 40 (Huene,1936), at least four preserve larger parts of the neural spines, that are just as robust, if not slightly more robust, than the spines of the lumbars in GSN F315. However, they differ in their orientation, which is more dorsal in GPIT 40 and more posterior in GSN F315. GPIT 40 also preserves three sacral vertebrae with

neural spines (Huene, 1936), which are robust and directed posteriorly, as in GSN F315. The neural spines of UFRGS PV-0146-T are gradually inclining more backward (posteriorly), starting from the thirteenth pre-sacral vertebra (25-30˚) until the twenty-first pre-sacral (40-45˚), thereafter the spines become less inclined until the twenty-sixth, at which it is almost vertical, a condition that also seems to be the case for the sacrals (Oliveira *et al*., 2009). In GSN F315 the lumbar and sacral neural spines are slightly posteriorly oriented (~70˚). All neural spines of the pre-sacral described by Oliveira *et al*. (2009), except for the axis, exhibit a slender morphology (i.e., anteroposteriorly narrow), whereas in GSN F315 two lumbar vertebrae preserve spines that are anteroposteriorly long, with a broad base and thinner towards the apex. Two of the three preserved sacral spines in GSN F315, are just as tall and robust as those of the preceding lumbar vertebrae. Von Huene (1936) described only three sacral vertebrae for GPIT 40, but the postcranial material for this specimen is preserved in disarticulation and considering evidence presented by the Namibian specimen, it is clear that there were more sacral elements. According to Oliveira *et al*. (2009) UFRGS PV-0146-T preserves four sacral vertebrae. However, in their figure 7, the position of the twenty-sixth presacral vertebra is well in the middle of the iliac blade and therefore it is here interpreted as another sacral vertebra, increasing the number of sacrals to five, the same number as in GSN F315.

5.1.1.2. Ribs

All ribs preserved for GSN F315 lack costal plates, a condition also represented in the South American chiniquodontids (MCZ 3781 and MCZ 4002; Romer and Lewis, 1973; UFRGS PV-0146-T; Oliveira *et al*., 2009, see Fig. 25). These plates are known in other cynodonts, like *Cynognathus*, *Diademodon*, *Thrinaxodon* and *Galesaurus* (Jenkins, 1971; Butler, 2009). A series of thoracic ribs in GSN F315 show a strong curvature immediately

following the head (Fig 25 A, B; arrows), a condition not observed in the ribs of specimens from South America. Post-mortem deformation is ruled out as both ribs displaying the pronounced curvature have been preserved on top of another. The sacral ribs are distally expanded in GSN F315 and MCZ 4002 (Romer and Lewis, 1973), to contact the iliac blade. Oliveira *et al*. (2009) describe the shapes of the distal articular surfaces of the four sacrals in UFRGS PV-0146-T as quadrangular and rectangular. In GSN F315 the distal articular surfaces of the sacral ribs are expanded to form mostly triangular or spoon-shaped morphologies, whereas the sacral vertebrae described by Huene (1936) for GPIT 40 also display a triangular expanded shape of the distal margin in dorsal view.

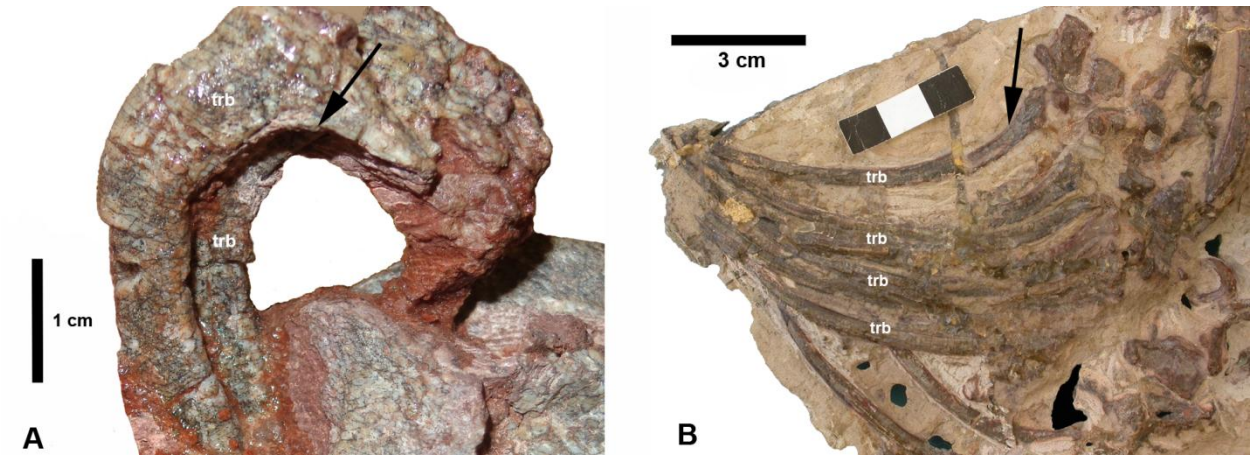

Figure 25. A, GSN F315 thoracic ribs in lateral view showing a strong curvature following immediately after the head; B, thoracic ribs of MCZ 4002 in lateral view. Abbreviations: trb, rib.

5.1.1.3. Shoulder girdle and clavicle

The slender right scapular blade of GSN F315 displays no sharp lateral flexure of the cranial and caudal borders, and has the distal portion of the scapular blade expanded. This same overall slender shape of the scapular blade has been shown for MCZ 4002 and MCZ 4164 from the Chañares Formation of Argentina (Romer and Lewis, 1973), and both MCZ 3616 (Romer, 1969a) and GPIT 40 (Huene, 1936) from the Santa Maria Formation of Brazil

(Fig. 26). Only one scapular blade from the Brazilian material is well preserved (MCZ 3616; 1969: fig. 9) and shows a very similar pattern in the development of the blade and acromion process to that of GSN F315. The scapula illustrated by Romer and Lewis (1973: fig. 7) is obviously incomplete, as also mentioned by these authors, evidently lacking the entire anterior margin where the acromion process should be represented. Similarities however are clear in the strong ridges developed in the anterior and posterior margins of the blade and the deeply concave morphology of the blade (Romer, 1969a; Romer and Lewis, 1973). GSN F315 preserves a large acromion process well above the neck of the scapula, which is also observed in South American chiniquodontids (e.g. MCZ 3616, MCZ 4164 and GPIT 40).

Romer and Lewis (1973) suggested that there was little acromial development in the scapular blade of MCZ 3801 from Argentina, although they report that the scapula was ventrally incomplete. The size of the acromion process in other cynodonts, like *Cynognathus*, *Diademodon* and *Thrinaxodon* is smaller and positioned on the neck of the scapula. The procoracoid in most South American chiniquodontis is either only partially or not preserved. As illustrated by Romer (1969a) the procoracoid of MCZ 3616 appears to be proportionally smaller than that of GSN F315, but first hand examination of the specimen from Brazil shows that the procoracoid is incompletely preserved (Fig. 26 C). The procoracoid of MCZ 3616 has a large, rounded foramen, which is laterally directed, whereas the procoracoid foramen in GSN F315, which is also large, is ellipsoid and directed laterally. The procoracoid in GSN F315 has a general rounded shape in lateral view a condition similar, although more pronounced in GPIT 40 (Huene, 1936), although it may have been affected by compression. The morphology of this bone in MCZ 4164 is more angular in lateral view (Romer and Lewis, 1973: fig. 14), showing a straight dorsoventral margin forming angles close to 90˚ with the upper and lower margins of the bone. GPIT 40 preserves a small, round procoracoid foramen (Huene, 1936).

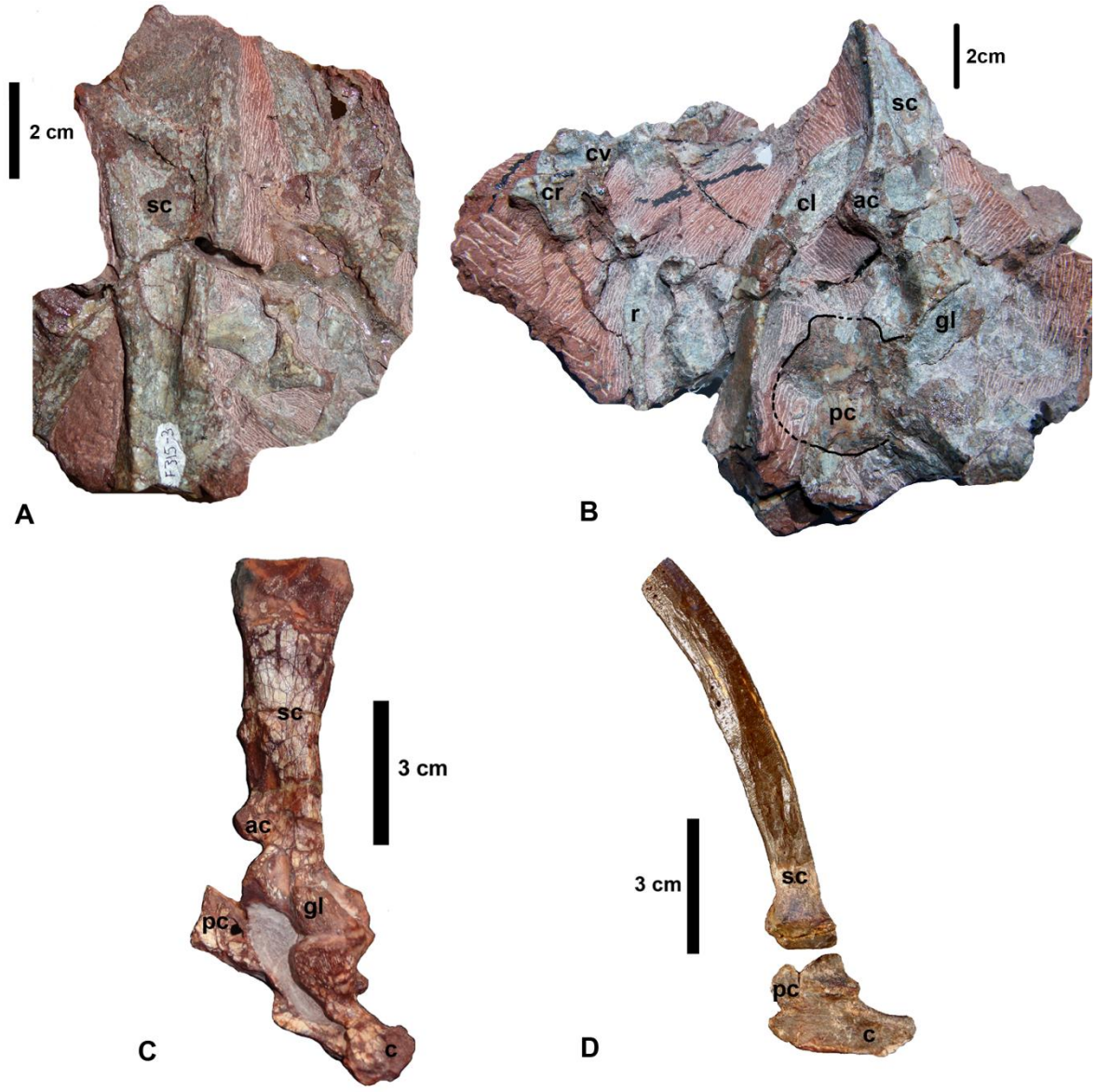

Figure 26. A, GSN F315 incomplete right scapula, lateral view; B, lateral view of GSN F315 incomplete left scapula with procoracoid; C, MCZ 3616 incomplete right scapula with partial procoracoid and coracoids, lateral view; D, MCZ 4002 with partial procoracoid and complete coracoids in lateral view. Abbreviations: sc, scapula; ac, acromion process; cl, clavicle; gl, glenoid; pc, procoracoid; c, coracoid; cv, cervical vertebra; cr, cervical rib; r, rib.

Romer and Lewis (1973: fig. 7) illustrate the pectoral girdle of *Chiniqodon* as having presenting an anteroposteriorly long and dorso-ventrally low procoracoid (these elements are attributed to MCZ 3781, but the illustrated coracoid and procoracoid are in fact part of MCZ

4002). First hand observation of MCZ 4002 however, shows that the anterior portion of the procoracoid is reconstructed (Fig. 27) and, considering current evidence, this bone is taller and shorter than the way it was portrayed by Romer and Lewis (1973) and its, antero- and slightly dorsal orientation is also inaccurate (see Romer and Lewis, 1973: fig. 7).

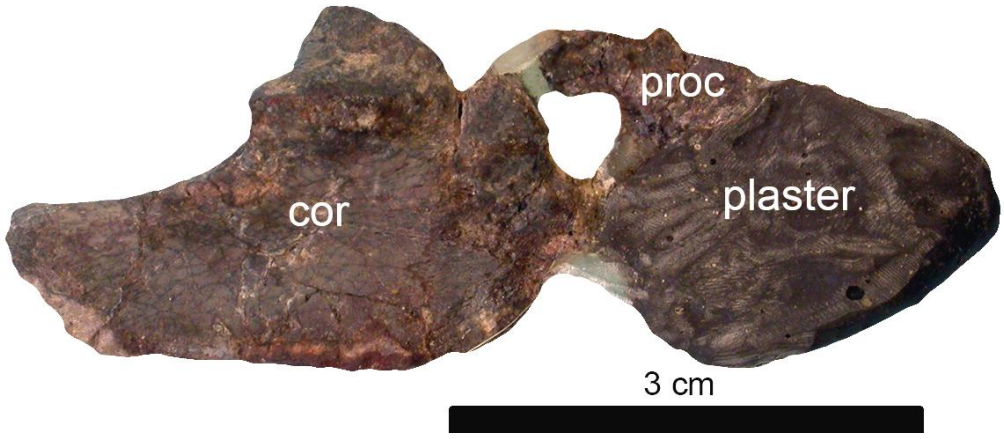

Figure 27. A, MCZ 4002 coracoid and procoracoid in lateral view from the Chañares Formation. Abbreviations: cor, coracoid; proc, procoracoid.

The clavicle of GSN F315 displays a much more gentle curvature (i.e., closer to 180˚) of ~145˚ between its proximal and distal end compared to the 138˚ curve angle of the clavicle of MCZ 4002 from the Chañares Formation (Fig. 28 A, B). The slight difference in curvature of 7˚ may be due to deformation in the specimen. Both MCZ 4002 (Romer and Lewis, 1973) and GSN F315 show the same dorsal deeply concave and expanded proximal margin for the attachment of the acromion.

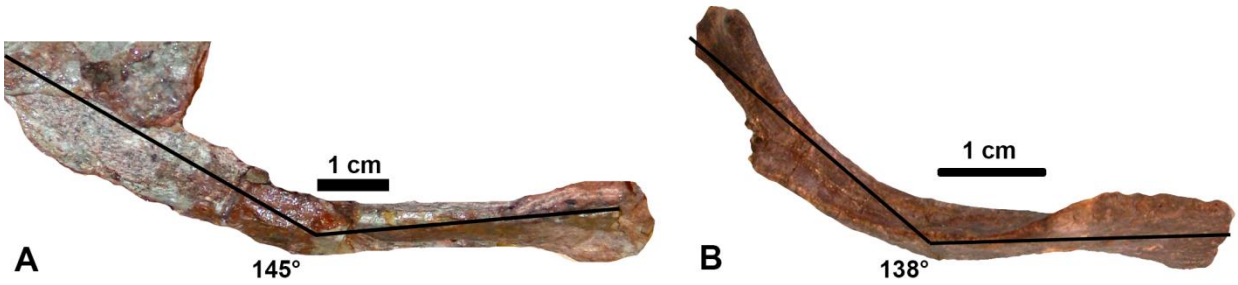

Figure 28. Dorso-lateral view of clavicles of A, GSN F315 and B, MCZ 4002.

5.1.1.4. Manus

Published descriptions of the manus in chiniquodontids is limited to the account of Romer and Lewis (1973). They state the very poor preservation of both manus in MCZ 3781, reporting the presence of at least three distals, an average length of 18 mm for metacarpals II-V and the lack of vestigial "extra" (disc-like) phalanges. The partial manus of GSN F315 shows an average length of 20 mm for metacarpals II-V and the absence of disc-like phalanges is also evident. For this study the manus of the Namibian specimen was also compared with the disarticulated elements of specimen PVL 3820 from the Chañares Formation. The latter show proximal and intermediate phalanges as having a more developed proximal margin than distal, a condition not observed clearly in GSN F315, and the unguals seem to be stronger in the specimen from Argentina. Proportions between the central phalange and ungual in PVL 3820 varied between 0.61; 0.90; 0.93 and 0.98, whereas the ratio was 0.74 in the only digit of GSN F315 with these phalanges complete.

5.1.1.5. Pelvis

The anterior lamina in GSN F315 is much more elongated than the posterior lamina. The specimens MCZ 4002 and MCZ 3781 (right ilium on margin of slab), preserve ilia with a general slender morphology. However, in specimen MCZ 4002, the anterior lamina has been

united to the rest of the pelvis by a large portion of glue, making the morphology of the ilium unreliable (Fig. 29 C). For example it seems clear considering overall evidence, that the dorsal margin of the ilium is not concave.

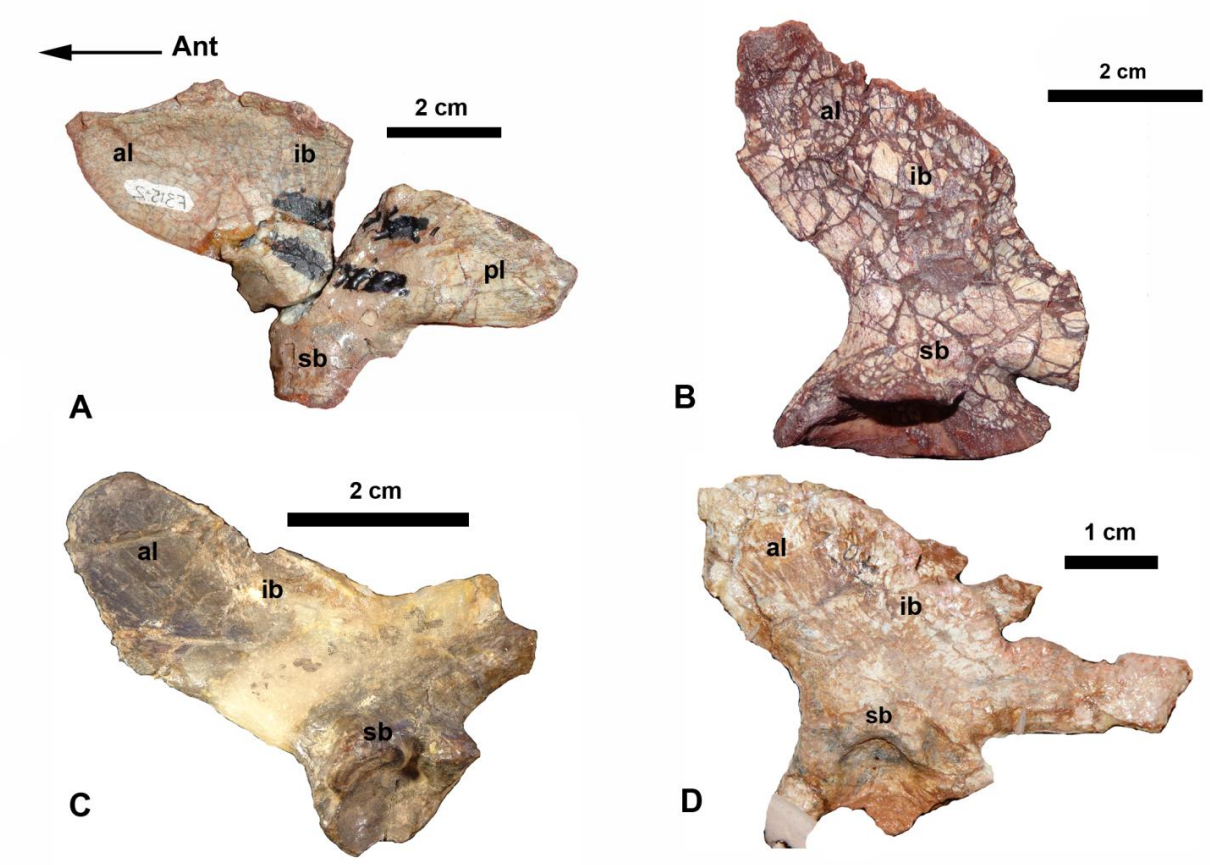

Figure 29. A, GSN F315 right ilium in lateral view (flipped); B, MCZ 3616 left ilium (lateral view); C, MCZ 4002 left ilium (lateral view); D, GPIT 40 right ilium in lateral view (flipped). Abbreviations: Ant, anterior; al, anterior lamina; pl, posterior lamina; ib, iliac blade; sb, supra-acetabular buttress.

Romer and Lewis (1973) interpreted a slender posterior lamina in specimens from Chañares and suggested a forward migration of the gluteal musculature, which is an advanced condition observed in mammals. The interpretation is more likely based on MCZ 4002, which, as mentioned above, has an important part of the ilium reconstructed and an incomplete posterior lamina. Evidence from GSN F315, as well as from Brazilian

chiniquodontids indicates that the posterior lamina continue to be high in this group (Fig. 29 A, B).

There is a wide angle between the edge of the posterior lamina and the margin of the neck in GSN F315, estimated at ~90˚. This angulation is much smaller in MCZ 3616 (Romer, 1969a), at ~20˚-30˚, although there is indeed considerable distortion in this specimen (Fig. 29 B). In GPIT 40, this angulation seems to be more similar to that observed in the Namibian specimen (Fig. 29 D). In MCZ 3616 (Romer, 1969a), GPIT 40 (Huene, 1936) and GSN F315 the supra-acetabular buttress is highly developed and does not project laterally, whereas the acetabular facet is directed ventrally. The neck of GSN F315 is much more robust than that in MCZ 4002 (Romer and Lewis, 1973, Fig. 29). GSN F315 is one of the few cynodonts showing nearly complete preservation of the fused pubo-ischium of both sides, other cases include *Cynognathus* (BMNH 2571) and the Brazilian *Trucidocynodon* (UFRGS-PV-1051-T; as represented by the preserved ischia). In small cynodonts, such as *Thrinaxodon* or *Galesaurus* these elements are not fused (Jenkins, 1971; Abdala, pers. com.). The acetabular foramen is well developed, apparently larger than in *Cynognathus*. The ischium in GSN F315 appears to be more developed than that illustrated by Romer and Lewis (1973: fig. 9) for specimens from Argentina, although the reconstruction presented by these authors should be considered with caution as it is based on the poorly preserved MCZ 3781.

5.1.1.6. Femur

The femora of GSN F315 and GPIT 40 are robust and short, contrasting with the slender condition of MCZ 3616 (Romer, 1969a; fig. 30 C). In MCZ 3616 the intertrochanteric fossa is a shallow and oval depression, whereas in GSN F315 it is a deep and rounded depression. In GSN F315 the lesser trochanter is more pronounced ventrally,

but in MCZ 3616 it is much longer, extending to nearly half the length of the bone. In MCZ 3616 and GSN F315 the lateral condyle is nearly double the size and protrudes more ventrally than the medial condyle (Fig. 30 D).

Figure 30. A, Lateral view of GSN F315 left femur; B, GPIT 40 left femur in lateral view; C, MCZ 3616 left femur in lateral view; D, GSN F315 right distal femur in antero-lateral view. Abbreviations: gt, greater trochanter; itf, intertrochanteric fossa; h, head; lt, lesser trochanter; lc, lateral condyle; mc, medial condyle; fo, fossa for the insertion of the adductor muscle.

Table 10. Proportions femur length/skull length in chiniquodontids and basal cynodonts (measurements in mm).

Specimen Number	Taxon	Skull length	Femur length	FL/SL
GSN F315	*Chiniquodon*	191	122	0.64
GPIT 40	*Chiniquodon*	260	162	0.62
UFRGS PV-0146-T	*Chiniquodon*	258	155	0.60
NMQR 3542	*Galesaurus*	103	61	0.59
TM 83	*Galesaurus*	93	58	0.62
OUMNH TSK 34	*Procynosuchus*	111	66	0.59
USNM 22812	*Thrinaxodon*	94	45	0.48
BP/1/1730	*Thrinaxodon*	79	44	0.56
BP/1/1730	*Thrinaxodon*	80	44	0.55
NMQR 809	*Thrinaxodon*	91	51	0.56

The femur of GSN 315 appears to be an extremely short and robust bone in comparison with other cynodonts. To investigate this issue the ratio of the femur to the length of the skull was compared amongst different basal cynodonts and chiniquodontid genera (Table 10). In basal cynodonts the ratio ranges between 0.48 and 0.62, whereas in chiniquodontid specimens it varies between 0.60 and 0.64. This ratio indicates that, contrary to the original intuition, the femur is longer in relation to the skull length in chiniquodontids than in any of the other cynodonts sampled.

5.1.1.7. Pes

The description presented here is the first account of elements from the pes in a chiniquodontid. Romer and Lewis (1973) mention the presence of poorly preserved elements

of the pes, without any particular description. GSN F315 show a remarkably large calcaneus with a tuber that is less differentiated that that illustrated by Jenkins (1971: fig. 60) for ?*Aleodon* or ?*Scalenodon*. The tuber in GSN F315 is certainly more similar to that of ?*Diademodon* (Jenkins, 1971: fig. 61). In *Trucidocynodon* the tuber is much larger and projected (Oliveira *et al*., 2010).

Comparison of metatarsals and metacarpals of GSN F315 show that the former are more robust and wider compared to the latter which are elongated and slender. This condition is reversed in cynodonts like *Thrinaxodon* in which the metacarpals and phalanges of the manus are more robust than those of the pes (Abdala, pers. com.).

5.1.2. Geology and environment of the Upper Omingonde Formation

Both sections, farms Okawaka and Omingonde comprise two architectural elements interpreted as overbanks (OF) and channels (CH). The sedimentology for the Omingonde section is more complex than that for Okawaka.

Farm Okawaka channel elements comprise litho-facies Gms which are interpreted as debris flow deposits (Miall, 1985) and the overbank elements comprise litho-facies Fl, interpreted as overbank mudstone deposits (Miall, 1985). Three channel elements (CH) and two overbank elements (OF) were identified and these elements alternate up-section. Architectural elements OF litho-facies Fl show the development of immature paleosols with greyish calcareous nodules and rhizocretions. Palaeosols may be identified based on the following characteristics; root traces (rhizocretions), soil structure and soil horizons (Retallack, 2001).

Farm Omingonde section comprises mostly mudstone and fine sandstone of channel and overbank architectural elements. Elements comprise a total of eight litho-facies Fr, Fl, Sp, Sh, Fm, Sl, Gm and Gms. Four channel elements comprise the following litho-facies combinations; CH1 litho-facies Sp is interpreted as linguoid transverse bars and Sh as a planar bed flow, CH2 litho-facies Fl is interpreted as representing a waning flood and Sl as either a scour fill or crevasse splay, CH3 litho-facies Gm is interpreted as a channel lag with the top litho-facies Fl interpreted as a waning flood deposit, and CH4 litho-facies Gms is interpreted as a debris flow deposit with load casts at the base of Gms deforming the top of litho-facies Sl (Miall, 1985). The load casts were formed as a result of compaction after deposition, resulting in deformation of the softer sediment below by the heavier sediment above. Three overbank architectural elements comprise the following; OF1 litho-facies Fr with the calcareous layers is interpreted as palaeosols and litho-facies Fl is interpreted as overbank and waning flood deposits, OF2 litho-facies Fm is interpreted as overbank deposits with the development of nodular, red-grey mottled immature palaeosols (Retallack, 2001) in which many vertebrate fossils have previously been found (Smith and Swart, 2002), and OF3 litho-facies Fl is interpreted as overbank and waning flood deposits.

The channel elements are much thicker on Farm Okawaka than those on Farm Omingonde, which may suggests that the source for the Okawaka deposits was more proximal. Previous studies done on the relative stability of mineral grains under weathering conditions in soils, suggest that K-feldspar, muscovite and quartz are the least easily weathered minerals (Retallack, 2001; fig. 4.4). The polymict conglomerates of the Okawaka channel deposits contain large pebbles of milky quartz and unweathered pink K-feldspar. Hydrolytic weathering causes the progressive reduction of alkali (Na^{+}, K^{+}) and alkaline earth (Ca^{2+}, Mg^{2+}) elements in soils that are formed in wet climates (Retallack, 2001). Therefore these elements may be more abundant in soils formed in arid climatic regimes during low

precipitation conditions. Petrographic analysis of the Okawaka deposits, show the presence of intact feldspar, which indicates very little chemical weathering typical of an arid climate with very little precipitation (Friedman *et al*., 1992). In addition to this unweathered state, the feldspar clasts are large in size (0.5-1.5 mm), which may indicate that the source of sediments was nearby. Milky quartz indicates a metamorphic origin, probably from the Damara basement or vein quartz. The conglomerate suggests a river channel deposit, most probably of a high-energy ephemeral river system. All measured channels dip towards the north. The sandstones and conglomerates form thick deposits which pinch out or interfinger laterally. This suggests rapid flash flood events and regular spill-over events. Mudstones represent overbank deposits.

Palaeocurrent measurements for the CH channel deposits of the Okawaka section, suggest that the provenance of the sediments is from a north-easterly located source. The petrographic results also suggest that the sediment did not travel far as 70% of the mineral grains are large, in the size class 1.5 mm and a large fraction of the mineral grains is represented by almost unaltered feldspars as well as pyroxene (53%). Pyroxene is an indicator of extreme immaturity. Previous studies have provided evidence for a meandering river system (Holzförster *et al.,* 1999; Wanke, 2000). Lower discharge rates favour meandering river systems and the development of palaeosols (Holzförster *et al.,* 1999).

The Upper Omingonde Formation on the Farm Omingonde, where GSN F315 and several other cynodonts were discovered, comprises conglomerates, sandstones, siltstones and palaeosols. The feldspar grains in the conglomerate have not been altered. This is very typical of arid environments, because breakdown of minerals needs the abundant and regular presence of moisture (Friedman *et al*., 1992). Thick sandstone and gritstone (quartz arenite) deposits alongside the river indicate river channels, with a southerly palaeocurrent direction. In places the arenite deposits interfinger with fine grained, red siltstone and lumpy palaeosols

of grey colour. The siltstones tend to be crumbly, with no evident structure in them and may have been blown in by the wind as they were previously described as loessites (Smith and Swart, 2002). These siltstones have yielded most of the vertebrate fossils (Keyser, 1973a, b, 1978).

Palaeocurrent measurements of the tabular cross-bedding observed in the fourth CH channel deposit of the Omingonde section, suggests a possible south-westerly sediment provenance. Visual observation of the rocks revealed the presence of angular <1.5cm pebbles. Petrographic results suggest that the sediment source may have been close by because 90% of the mineral grains are subangular, a large component comprises large mineral grains (0.5-2 mm), especially of feldspars and the texture consists of well sorted mineral grains. Palaeocurrent data and the architectural elements identified for the Omingonde farm field section, supports the presence of a braided river system for the Upper Omingonde, as tabular and cross laminations dip south to south-westerly, while the channels dip parallel to these in a southerly direction. Previous studies have provided evidence for a switch from a braided river system to a meandering river in the Upper Omingonde (Smith and Swart, 2002). High discharge rates favour braided river systems (Holzförster *et al.*, 1999).

The sedimentary rocks on the farms Omingonde and Okawaka were deposited near the Waterberg-Omaruru Fault Zone (Holzförster *et al.*, 1999; Wanke, 2000; Smith and Swart, 2002). The source of the igneous minerals in the Okawaka rocks was probably from the igneous Damara basement rocks and vein quartz (Holzförster *et al.*, 1999). The deposits on the farm Omingonde indicate occasional amalgamation of smaller channels and the deposition of thick overbank deposits, which may be interpreted as resulting from high subsidence rates in the tectonically active Waterberg Basin (Smith and Swart, 2002). Although the Okawaka deposits are much coaser than those from Farm Omingonde, the latter

is positioned more proximal to the Waterberg-Omaruru Fault (Holzförster *et al.*, 1999; Smith and Swart, 2002). Generally, the river channels carried loads of gritstone and finer muddy material, which was spilled over into the overbanks. During Upper Omingonde times terrestrial animals probably lived in the overbank environment as most of the better preserved vertebrate fossils of the Upper Omingonde Formation have been collected from thick pedogenically modified massive siltstone beds. These massive siltstones have been interpreted as loessites which were rapidly deposited by dust storms, and may have had a higher preservation potential due to increased rates of bone burial (Smith and Swart, 2002).

The deposits in which chiniquodontids have been collected in Argentina, Brazil and Namibia represent mostly fluvial and floodplain environments which were formed during arid climatic conditions. The Chañares Formation was deposited in an arid to semi-arid seasonal climate with a mean annual precipitation of 250-1500 mm (Curtin, 2001). Annual precipitation increased from 760 mm or less in the lower half of the Ischigualasto Formation to 760-2100 mm in the upper half of the formation demonstrating seasonal fluctuations between dry and wet climatic extremes (Shipman, 2004). Petrographic evidence from the Santa Maria Sequence 1 reveals a climatic seasonality trend with a shift to a somewhat wetter climatic phase, as shown by considerable meteoric water infiltration in sandstones, within an overall semiarid climate, characterised by high evaporation rates (Zerfass *et al.*, 2003).

Smith and Swart (2002) suggested that the Upper Omingonde had a general arid zone signature with groundwater levels fluctuating seasonally. Petrographic analysis performed during this study confirmed that the Upper Omingonde deposits were more likely deposited in an arid climatic regime, due to the high presence of almost unaltered feldspars and pyroxene. A shift took place from a semi-arid to a wetter climate causing a gradual switch from a single, wide and shallow braided system to a series of narrow meander belts separated and confined by extensive floodplains (Smith and Swart, 2002). This study found that the

depositional environments for both study areas preserved fluvial deposits, although the depositional environments varied, probably as a result of the interplay of various mechanisms and conditions, such as basin subsidence rates, sediment availability and location of the deposits in relation to the Waterberg-Omaruru Fault (Friedman, 1992; Boggs, 2006).

6. Chapter 6

6.1. Conclusion

The chiniquodontid material described from the Upper Omingonde Formation of Namibia was positively identified as *Chiniquodon* based on several skull features identified, such as, including a low arched zygoma, sectorial postcanines without serrations; and an elevated sagittal crest is in relation to the skull profile (Abdala and Giannini, 2002).

Chiniquodontid postcrania are characterized by the absence of costal plates on the ribs; expanded distal portions of the sacral ribs for the attachment to the ilium; tall and slender scapular blade; large acromion process positioned well above the scapular neck; proximal margin of the clavicle deeply concave and expanded; rounded shape of the procoracoid in lateral view; absence of disc-like phalanges in manus and pes; high posterior lamina of the ilium with a well-developed supra-acetabular buttress that does not project laterally; acetabular facet directed ventrally; robust femur with a ratio femur length/skull length of 0.60 to 0.64; femoral lateral condyle nearly double the size and protrudes more ventrally than the medial condyle.

Postcranial features that differentiate the Namibian *Chiniquodon* specimen from other chiniquodontids are: lumbar and sacral vertebral spines are more robust and orientated more posteriorly; thoracic ribs have a strong proximal curvature following the head (deformation ruled out); distal articular surfaces of the sacral ribs are triangular or spoon-shaped (also observed in one specimen from Brazil); in lateral view, the procoracoid is less rounded than that of other chiniquodontids with a large ellipsoid procoracoid foramen; the angle between the proximal and distal ends of the clavicle, is more gently curved at ~145˚ (although this may be due to post-mortem deformation); the unguals of the manus are not as strongly developed; the neck of the ilium is robust; the angulation between the edge of the posterior

lamina and the margin of the neck is large at ~90˚; and the ischium has a large ellipsoid obturator foramen and is more than twice the size of the pubic plate.

The discovery of *Chiniquodon* as well as the dicynodont, *Stahleckeria* and a rauisuchian archosaur in the Upper Omingonde Formation indicates that the formation has a Ladinian age (Abdala *et al*, 2013) and is thus younger than currently known Middle Triassic faunas from continental Africa. *Chiniquodon* from Namibia is the only Middle Triassic chiniquodontid known from the Middle Triassic of continental Africa.

This study confirmed the results of previous geological studies (Holzförster *et al.,* 1999; Wanke, 2000; Smith and Swart, 2002) that the Namibian *Chiniquodon* lived near fluvial environments, represented by braided and meandering rivers, in a predominately arid climatic regime.

7. References

Abdala, F., and Giannini, N.P., 2002. Chiniquodontid cynodonts: systematic and morphometric considerations. Palaeontology 45, 1151-1170.

Abdala, F., Martinelli, A.G., Bento Soares, M., de la Fuente M., and Ribeiro, A.M., 2009. South American Middle Triassic continental faunas with amniotes: biostratigraphy and correlation. 15th Biennial Meeting of the Palaeontological Society of Southern Africa, Palaeontologia africana, 44, 83-87.

Abdala, F., and Ribeiro, A.M., 2010. Distribution and diversity patterns of Triassic cynodonts (Therapsida, Cynodontia) in Gondwana. Palaeogeography, Palaeoclimatology, Palaeoecology 286, 202-217.

Abdala, F., and Smith, R.M.H., 2009. A middle Triassic cynodont fauna from Namibia and its implications for the biogeography of Gondwana. Journal of Vertebrate Paleontology 29, 837-851.

Abdala, F., Marsicano, A.M, Smith, R.M.H., and Swart, R., 2013. Strengthening western Gondwanan correlations: A Brazilian dicynodont (Synapsida, Anomodontia) in the Middle Triassic of Namibia. Gondwana Research 23, 1151-1162.

Alcober, O., 1996. Revisión de los crurotarsi, estratigrafía y tafonomía de la Formación Ischigualasto. Unpublished PhD Thesis, Universidad National de San Juan, San Juan, Argentina, 260 pp.

Barberena, M.C., 1977. Bioestratigrafia preliminar da Formação Santa Maria. Pesquisas, 7, 111-129.

Benton, M.J., and Twitchett, R.J., 2003. How to kill (almost) all life: the end-Permian extinction event. Trends in Ecology & Evolution, 18, 7, 358-365.

Besairie, H., 1953. Geologie de Madagascar; Le sud du bassin de Morondava. Travaux du Bureau Géologique, Madagascar, No. 44.

Blackburn, T.J., Olsen, P.E., Bowring, S.A., McLean, N.M., Kent, D.V., Puffer, J., McHone, G., Rasbury, T., and Et-Touhami, M., 2013. Zircon U-Pb geochronology links the end-Triassic extinction with the Central Atlantic Magmatic Province. Science, 340, 941-945.

Boast, J., and Nairn, A.E.M., 1982. An outline of the geology of Madagascar. Chapter 14, 649-696. In: Nairn, A.E.M., and Stehli, F.G., (eds.). The Ocean Basins and Margins. Plenum Press, New York, 776 pp.

Boggs, Jr. S., 2006. Principles of Sedimentology and Stratigraphy. Fourth Edition. Pearson Prentice Hall, New Jersey, 662 pp.

Bonaparte, J.F., 1966. *Chiniquodon* Huene (Therapsida, Cynodontia) en el Triásico de Ischigualasto, Argentina. Acta Geológica Lilloana, 8, 157-169.

Bonaparte, J.F., 1982. Faunal replacement in the Triassic of South America. Journal of Vertebrate Paleontology 2, 362-371.

Bonaparte, J.F., 1997. El Triassico de San Juan-La Rioja Argentina y sus dinosaurios. Museo Argentino de Ciencias Naturales, Buenos Aires, 174 pp.

Butler, E., 2009. The postcranial skeleton of the Early Triassic non-mammalian cynodont *Galesaurus planiceps*: implications for biology and lifestyle. Unpublished MSc Thesis, University of the Free State, Bloemfontein, South Africa, 153 pp.

Caselli, A.T., 1998. Estratigrafía y sedimentología de las formaciones Patquía (Pérmico) y Talampaya (Triásico inferior) en las Sierras Pampeanas Noroccidentales y Precordillera Central (provincias de La Rioja y San Juan). Unpublished PhD Thesis, Universidad de Buenos Aires, Buenos Aires, Argentina, 437 pp.

Catuneanu, O., Wopfner, H., Eriksson, P.G., Cairncross, B., Rubidge, B.S., Smith, R.M.H., and Hancox, P.J., 2005. The Karoo basins of south-central Africa. Journal of African Earth Sciences 43, 211-253.

Cohen, K.M., Finney, S.C, Gibbard, P.L., and Fan, J.-X., 2013, updated. The ICS International Chronostratigraphic Chart. Episodes 36, 199-204.

Currie, B.S., Colombi, C.E., Tabor, N.J., Shipman, T.C., and Montañez, I.P., 2009. Stratigraphy and architecture of the Upper Triassic Ischigualasto Formation, Ischigualasto Provincial Park, San Juan, Argentina. Journal of South American Earth Sciences, 27, 74-87.

Curtin, T.M., 2001. Linking time-equivalent paleosols and lacustrine rocks to reconstruct paleoclimate in the Ischigualasto basin, NW Argentina. Unpublished PhD Thesis, University of Arizona, Tucson, AZ, 173 pp.

Erickson, J. 2002. Historical Geology, Understanding Our Planet's Past. Facts on File Inc, 307 pp.

Erwin, D.H., 1990. The end Permian mass extinction. Annual Review of Ecology and Systematics, 21, 69-91.

Friedman, G.M., Sanders, J.H., and Kopaska-Merkel, D.C., 1992. Principles of Sedimentary Deposits. Stratigraphy and Sedimentology. Macmillan Publishing Company, New York, 717 pp.

Gevers, T.W., 1936. The Etjo Beds of Northern Hereroland, South West Africa. Transactions of the Geological Society South Africa, 39, 317-329.

Gyllenhaal, E.D., 1990. Calibration of geologic indicators of moisture regime in the tropics and subtropics. Paleogeographic Atlas Project, First annual meeting, 40-45.

Holzförster, F., Stollhofen, H., and Stanistreet, I.G., 1999. Lithostratigraphy and depositional environments in the Waterberg-Erongo area, central Namibia, and correlation with the main Karoo Basin, South Africa. Journal of African Earth Sciences, Vol. 29, .105-123.

Hopson, J.A., and Kitching, J.W., 1972. A revised classification of cynodonts (Reptilia: Therapsida). Palaeontologia africana, 14, 71-85.

Hopson, J.A., and Kitching, J.W., 2001. A probainognathian cynodont from South Africa and the phylogeny of non-mammalian cynodonts. Bulletin for the Museum of Comparative Zoology, 156, 5-35.

Huene von, F., 1936. Die fossilen Reptilien des südamerikanischen Gondwanalandes. Ergebnisse der Sauriergrabungen in Südbrasilien 1928-29. Lieferung 2, Tübingen: Franz F. Heine, 93-159.

Ianuzzi, R., and Schultz, C.L., 1997. Primeiro registro de megafósseis vegetais no Membro Alemoa da Formação Santa Maria, RS (Triássico Médio a Superior). Congreso Brasileiro de Paleontología, 15, 35.

Kammerer, C.F., Flynn, J.J., Ranivoharimanana, L., and Wyss, A.R., 2010. The first record of a probainognathian (Cynodontia: Chiniquodontidae) from the Triassic of Madagascar. Journal of Vertebrate Paleontology, 30, 1889-1894.

Kemp, T.S., 2005. The origin and evolution of mammals. Oxford University Press, Oxford, UK, 331pp.

Keyser, A.W., 1973a. A new Triassic vertebrate fauna from South West Africa. Palaeontologia africana, 16, 1-15.

Keyser, A.W., 1973b. New Triassic vertebrate fauna from South West Africa. South African Journal of Sciences, 69, 113-115.

Keyser, A.W., 1978. A new bauriamorph from the Omingonde Formation (Middle Triassic) of South West Africa. Palaeontologia africana, 21, 177.

Kielan-Jaworowska, Z., Cifelli, R.L., and Luo., Z.X., 2004. Mammals from the age of dinosaurs: origins, evolution, and structure. Columbia University Press, New York, 630pp.

Kitching, J.W., 1995. Biostratigraphy of the *Cynognathus* Assemblage Zone. 40–45. In: Rubidge, B. S., (ed.). Biostratigraphy of the Beaufort Group (Karoo Supergroup). Series 1, South African Committee for Stratigraphy, Pretoria, 46pp.

Kokogian, D.A., Spalletti, L.A., Morel, E.M., Artabe, A.E., Martínez, R.N., Alcober, O.A., Milana, J.P., and Zavattieri, A.M., 2001. Estratigrafía del Triásico argentino. In: Artabe A.E., Morel, E.M., and Zamuner, A.B., (eds.). El Sistema Triásico en la Argentina, 23-54. Fundación Museo de La Plata 'Francisco Pascasio Moreno', La Plata, Argentina.

Langer, M.C., 2005. Studies on continental Late Triassic tetrapod biochronology. II. The Ischigualastian and a Carnian global correlation. Journal of South American Earth Sciences, 19, 219-239.

Langer, M., Boniface, M., Cuny, G., and Barbieri, L., 2000. The phylogenetic position of *Isalorhynchus genovefae*, a Late Triassic rhynchosaur from Madagascar. Annales de Paléontologie 86, 2, 101-127.

López Gamundí, O.R., Alvarez, L., Andreis, R.R., Bossi, G.E., Espejo, I.S., Fernandez Seveso, F.F., Legaretta, L., Kokogian, D.A., Limarino, C.O., and Sessarego, H.L., 1989. Cuencas intermontanas. Correlación Geológica, 6, 123-167.

Lucas, S.G., 1998. Global Triassic tetrapod biostratigraphy and biochronology. Palaeogeography, Palaeoclimatology, Palaeoecology, 143, 347-384.

Machado, C.B., 2004. Concentrações fossilíferas controladas pelo nível freático: um modelo tafonômico para reconstruções paleoambientais. Programa de Pós-graduação Geosciências Universidade Federal do Rio Grande do Sul, Dissertação de Mestrado, 73pp.

Mancuso, A.C., 2005a. Tafonomía en ambientes lacustres: estudio integral de las sociaciones fósiles de las secuencias lacustres del Triásico Medio de la Cuenca de Ischigualasto-

Villa Unión (formaciones Chañares, Los Rastros e Ischichuca). Unpublished PhD Thesis, Universidad de Buenos Aires, Buenos Aires, Argentina, 208 pp.

Mancuso, A.C., 2005b. Revisión y aportes a la estratigrafía de la sección inferior del Grupo Agua de la Peña (Triásico Medio, Argentina). XVI Congreso Geológico Argentino, La Plata, Argentina, Actas 3, 415-422.

Mancuso, A.C., and Caselli, A.T., 2012. Paleolimnology evolution in rift basins: the Ischigualasto-Villa Unión Basin (Central-Western Argentina) during the Triassic. Sedimentary Geology, 275-276, 38-54.

Mancuso, A.C., Gaetano, L.C., Leardi, J.M., Abdala, F., and Arcucci, A.B., 2014. The Chañares Formation: a window to a Middle Triassic tetrapod community. Lethaia, 47, 244-265.

Martin, H., 1961. The hypothesis of continental drift in the light of recent advances of geological knowledge in Brazil and in South West Africa. The Geological Society of South Africa, Alexander L. du Toit Memorial Lectures, Vol. 7, The Geological Society of South Africa, Johannesburg, 1-47.

Martínez, R.N., and Forster, C.A., 1996. The skull of *Probelesodon sanjuanensis*, sp. nov., from the Late Triassic Ischigualasto Formation of Argentina. Journal of Vertebrate Paleontology, 16, 285-291.

Martínez, R.N., May, C.L., and Forster, C.A., 1996. A new carnivorous cynodont from the Ischigualasto Formation (Late Triassic, Argentina), with comments on Eucynodont Phylogeny. Journal of Vertebrate Paleontology, 16, 2, 271-284.

Martínez, R.N., Sereno, P.C., Alcober, O.A., Colombi, C.E., Renne, P.R., Montañez, I.P., and Currie, B.S., 2011. A basal dinosaur from the dawn of the dinosaur era in southwestern Pangaea. Science, 331, 201-210.

Martínez, R.N., Fernandez, E., and Alcober, O.A., 2013. A new Non-Mammaliaform Eucynodont from the Carnian-Norian Ischigualasto Formation, Northwestern Argentina. Revista Brasileira De Paleontologia, 16, 1, 61-76.

Miall, A.D., 1977. A review of the braided-river depositional environment. Earth-Science Reviews, 13, 1-62.

Miall, A.D., 1985. Architectural-element analysis: A new method of facies analysis applied to fluvial deposits. Earth Science Reviews, 22, 261-308.

Miall, A.D., 2000. Principles of sedimentary basin analysis. 3rd Edition, Springer, 616pp.

Milana, J.P., and Alcober, O., 1994. Modelo tectonosedimentario de la cuenca triásica de Ischigualasto (San Juan, Argentina). Revista de la Asociación Geológica Argentina, 49, 217-235.

Odin, G.W., and Letolle, R., 1982. The Triassic time scale in 1981. In: Odin, G.S., (ed.). Numerical Dating in Stratigraphy. John Wiley and Sons, Chichester, UK, 523-533.

Oliveira, T.V., Bento Soares, M., and Schultz, C.L., 2010. *Trucidocynodon riograndensis* gen. nov. et sp. nov. (Eucynodontia), a new cynodont from the Brazilian Upper Triassic (Santa Maria Formation). Zootaxa, 2382, 1-71.

Oliveira, T.V., Schultz, C.L., and Bento Soares, M., 2009. A partial skeleton of *Chiniquodon* (Cynodontia, Chiniquodontidae) from the Brazilian Middle Triassic. Revista Brasileira De Paleontologia, 12, 2, 113-122.

Porada, H., Löffler, T., Horsthemke, E., Ledendecker, S. and Martin, H., 1996. Facies and palaeoenvironmental trends of northern Namibian Karoo sediments in relation to West Gondwanaland palaeogeography. Proceedings 9th International Gondwana Symposium, Hyperabad/India, Vol. 2, Oxford and IBH Publishing, 1101-1114.

Retallack, G.J., 2001. Soils of the past, An introduction to paleopedology, 2nd Edition. Blackwell Science, Oxford, UK, 404pp.

Retallack, G.J., Metzger, C.A., Jahren, A.H., Greaver, T., Smith, R.M.H., and Sheldon, N.D, 2006. Middle-Late Permian mass extinction on land. GSA Bulletin, 118, 1398-1411

Reuning, E., and von Huene, F., 1925. Fossilführende Karroo-schichten im nördlichen S.W.A. Neues Jahrbuch für Mineralogie, Geologie und Paläontologie, Abteilung B, Beilage-Band 52, 94-l22.

Rogers, R.R, Arcucci, A.B, Abdala, F., Sereno, P.C., Forster, C.A., and May, C.L., 2001. Paleoenvironment and Taphonomy of the Chañares Formation Tetrapod Assemblage (Middle Triassic), Northwestern Argentina: Spectacular Preservation in Volcanogenic Concretions. Palaios, 16, 461-481.

Rogers, R.R., Swisher, C.C., Sereno, P.C., Monetta, A.M., Forster, C.A., and Martínez, R.N., 1993. The Ischigualasto tetrapod assemblage (Late Triassic, Argentina) and 40Ar-39Ar dating of dinosaur origins. Science, 260, 794-797.

Romer, A.S., 1969a. The Brazilian Triassic cynodont reptiles *Belesodon* and *Chiniquodon*. Breviora 332, 1-16.

Romer, A.S., 1969b. The Chañares (Argentina) Triassic reptile fauna. V. A new chiniquodontid cynodont, *Probelesodon lewisi*. Cynodont ancestry. Breviora, 333, 1-24.

Romer, A.S., 1970. The Chanares (Argentina) Triassic reptile fauna VI: A chiniquodontid cynodont with an incipient squamosal-dentary jaw articulation. Breviora, 344, 1-18.

Romer, A.S., 1973. The Chañares (Argentina) triassic reptile fauna. XVIII. *Probelesodon minor*, a new species of carnivorous cynodont. Familia Probainognathidae. Breviora, 401, 1-4.

Romer, A.S., and Jensen, J.A., 1966. The Chañares (Argentina) Triassic reptile fauna. II. Sketch of the geology of the Río Chañares-Río Gualo region. Breviora, 252, 1-20.

Romer, A.S. and Lewis, A.D., 1973. The Chanares (Argentina) Triassic reptile fauna. XIX. Postcranial materials of the cynodonts *Probelesodon* and *Probainognathus*. Breviora, 407, 1-26.

Rubert, R.R., and Schultz, C.L., 2004. Um novo horizonte de correlação para o Triássico Superior do Rio Grande do Sul. Pesquisas em Geociências, 31, 71-88.

Rubidge, B. S. (ed.). 1995. Biostratigraphy of the Beaufort Group (Karoo Supergroup). Council for Geoscience, South African Committee for Stratigraphy, Biostratigraphic Series 1, 46pp.

Rubidge, B.S., 2013. The roots of early mammals lie in the Karoo: Robert Broom's foundation and subsequent research progress. Transactions of the Royal Society of South Africa 68, 41-52.

Rubidge, B.S., and Sidor, C.A., 2001. Evolutionary patterns among Permo-Triassic therapsids. Annual Review of Ecology and Systematics, 449-480.

Scherer, C.M.S., Faccini, U.F., Barberena, M.C., Schultz, C.L., and Lavina, E.L., 1995. Bioestratigrafia da Formação Santa Maria: utilização das cenozonas como horizontes de correlação. Comunicações do Museu de Ciências e Tecnologia UBEA/PUCRS, Série Ciências da Terra 1. Sociedade Brasileira de Geologia, 33-42.

Schultz, C.L., Scherer, C.M.S., and Barberena, M.C., 2000. Biostratigraphy of Southern Brazilian Middle–Upper Triassic. Revista Brasileira de Geociências, 30, 3, 491-494.

Shipman, T.C., 2004. Links between sediment accumulation rates and the development of alluvial architecture: Triassic Ischigualasto Formation, northwestern Argentina. Unpublished PhD Thesis, University of Arizona, Tucson, AZ, 243 pp.

Smith, A.G., 1999. Gondwana: its shape, size and position from Cambrian to Triassic times. Journal of African Earth Sciences, Vol. 28, No. 1, 71-97.

Smith, R.M.H., Eriksson, P. G., and Botha, W.J., 1993. A review of the stratigraphy and sedimentary environments of the Karoo-aged basins of southern Africa. Journal of African Earth Sciences, 16, 143-169.

Smith, R.M.H., and Swart, R., 2002. Changing fluvial environments and vertebrate taphonomy in response to climatic drying in a Mid-Triassic rift valley fill: the Omingonde Formation (Karoo Supergroup) of central Namibia. Palaios 17, 249-267.

Spalletti, L.A., Artabe, A., Morel, E., and Brea, M., 1999. Biozonación paleoflorística y cronoestratigrafia del Triásico argentino. Ameghiniana 36, 419-451.

Stipanícic, P.N., 1983. The Triassic of Argentina and Chile. In: Moullade, M., and Nairn, A.E.M., (eds.). The Phanerozoic Geology of the World. The Mesozoic, Elsevier Press, Amsterdam, 181-199.

Stipanícic, P.N., and Marsicano, C.A., 2002. Triásico. In Léxico estratigráfico de la Argentina. Volumen VIII. Asociación Geológica Argentina, Serie B (Didáctica y Complementaria) 26, 370 pp.

Tanner, L.H., and Hubert, J.F., 2001. Stability of atmospheric CO_2 levels across the Triassic/Jurassic boundary. Nature, 411, 6838, 675-677

Teixeira, A.M.S., 1982. Um novo cinodonte carnívoro (*Probelesodon kitchingi*, sp. nov.) do Triássico do Rio Grande do Sul, Brasil. Comunicações do Museu de Ciencias PUCRGS 24, 1-31.

Tucker, M.E. and Benton, M.J., 1982. Triassic environments, climates and reptile evolution. Palaeogeography, Palaeoclimatology, Palaeoecology, 40, 361-379.

Veevers, J.J., 2004. Gondwanaland from 650–500 Ma assembly through 320 Ma merger in Pangea to 185–100 Ma breakup: supercontinental tectonics via stratigraphy and radiometric dating. Earth Science Reviews 68, 1-132.

Wanke, A., 2000. Karoo-Etendeka unconformities in NW Namibia and their tectonic implications. Unpublished PhD Thesis, Bayerischen Julius-Maximilians-Universität Würzburg, 114 pp.

Ward, P.D., Montgomery, D.R., and Smith, R. 2000. Altered river morphology in South Africa related to the Permian–Triassic extinction. Science, 289, 1740-1743.

Zerfass, H., Lavina, E.L., Schultz, C.L., Garcia, A.J.V., Faccini, U.F., and Chemale, F. Jr., 2003. Sequence stratigraphy of continental Triassic strata of southernmost Brazil: a contribution to southwestern Gondwana palaeogeography and palaeoclimate. Sedimentary Geology 161, 85-105.

Zerfass, H., Chemale, F. Jr., Schultz, C.L., and Lavina, E., 2004. Tectonics and sedimentation in southern south America during Triassic. Sedimentary Geology 166, 265-292.

8. Appendix 1.

Petrographic results of farms Okawaka and Omingonde

Sample OKO 1

I. Formation name, geographic location, architectural element
Upper Omingonde Formation; Farm Okawaka; OF overbank mudstone fines
II. Texture
A. Grain size and sorting
- *20-180 µm*
- *well sorted*

B. Grain shape
- *subrounded (60%) & subangular (40%)*

C. Stage of textural maturity
- *immature*

D. Fabric
- *flat muscovite plate, fibrous biotite strings, subangular quartz grains, subangular* orthoclase, subrounded pyroxene
- *Matrix : grains 20 : 80 = grain supported*
- *grains very closely packed: point contacts (40%)* & *concavo-convex contacts (60%)*
- *30% depositional porosity* (i.*e. pore-filling cement plus current porosity)*

III. Mineral composition
Grains:
1. Percentage of quartz: 85%
   - *monocrystalline 100% vs. polycrystalline 0%*
   - *undulatory 80% vs. non-undulatory 20%*
   - *grain size 20 µm - 150 µm very fine sand*
2. Percentage of mica: 2%
   - *muscovite & biotite*
   - *grain size 10-20 µm*
3. Percentage of other terrigenous minerals: <25 %
   - *feldspars*, orthoclase, pyroxene, microcline
   - *grain size 10-150 µm (very fine sand)*

IV. Diagenetic features
- *calcite cement*
- *Fe-oxides present as tiny* red *specs*

V. Classification
- *siltstone*

Sample OKO 2

I. Formation name, geographic location, architectural element
Upper Omingonde Formation; Farm Okawaka; CH channel deposits
II. Texture
A. Grain size and sorting
- *0.5-1.5 mm*

- *moderately sorted*

B. Grain shape
- *subrounded (50%) & subangular (50%)*

C. Stage of textural maturity
- *immature*

D. Fabric
- *flat mica plates* & *subangular to subrounded quartz grains -*
- *matrix : grains 5 : 95 = grain supported*
- *grains very closely packed: point contacts (40%)* & *concavo-convex contacts (60%)*
- *5% depositional porosity* (i.*e. pore-filling cement plus current porosity)*

III. Mineral composition

Grains:

1. Percentage of quartz: 45%
   - *monocrystalline 100% vs. polycrystalline 0%*
   - *undulatory 80% vs. non-undulatory 20%*
   - *grain size 0.25-1.25 mm*
2. Percentage of mica: <2%
   - *muscovite*
   - *grain size 0.2-0.5 mm*
3. Percentage of other terrigenous minerals: 53 %
   - *orthoclase (90%) and microcline(10%)*
   - *grain size 0.5-1.5 mm*

IV. Diagenetic features
- *calcite cement*
- *Haematite grains present as minute grains*

V. Classification
- ❖ *sandstone*

Sample OMI 1

I. Formation name, geographic location, architectural element

Upper Omingonde Formation; Farm Omingonde; OF1 overbank siltstone fines

II. Texture

A. Grain size and sorting
- *20-200 µm*
- *poorly sorted*

B. Grain shape
- *subrounded (60%) & subangular (40%)*

C. Stage of textural maturity
- *mature*

D. Fabric
- *flat mica plates, elongated mica strings* & *subangular and subrounded quartz grains -*
- *matrix : grains 80 : 20* = matrix *supported*
- *grains very loosely packed, surrounded by calcitic matrix*
- *70% depositional porosity* (i.*e. pore-filling cement plus current porosity)*

III. Mineral composition

Grains:

1. Percentage of quartz: 85%

- *monocrystalline 100% vs. polycrystalline 0%*
- *undulatory 80% vs. non-undulatory 20%*
- *grain size 10-200 µm*

2. Percentage of mica: <2%
   - *biotite & muscovite*
   - *grain size 10-500 µm*
3. Percentage of other terrigenous minerals: <15 %
   - *orthoclase, other feldspars*
   - *grain size 10-200 µm*

IV. Diagenetic features
- *calcite cement*

V. Classification
- *siltstone*

Sample OMI 2

I. Formation name, geographic location, architectural element

Upper Omingonde Formation; Farm Omingonde; OF1 overbank siltstone fines

II. Texture

A. Grain size and sorting
- *20-200 µm*
- *moderately sorted*

B. Grain shape
- *subrounded (80%) & subangular (20%)*

C. Stage of textural maturity
- *mature*

D. Fabric
- *rounded structures of calcareous rootlets*
- *matrix : grains 90 : 10 = matrix supported*
- *grains very loosely distributed*
- *70% depositional porosity* (i.*e. pore-filling cement plus current porosity)*

III. Mineral composition

Grains:

1. Percentage of quartz: 50%
   - *monocrystalline 100% vs. polycrystalline 0%*
   - *undulatory 80% vs. non-undulatory 20%*
   - *grain size 2-200 µm*
2. Percentage of mica: <1%
   - *biotite, muscovite*
   - *grain size 20-200 µm*
3. Percentage of other terrigenous minerals: <1 %
   - *feldspars, chloritoids*
   - *grain size 10-100 µm*

IV. Diagenetic features
- *calcite cement (50%)*
- *chloritoid* and haematite blebs & *crystals*

V. Classification
- *siltstone*

Sample OMI 3

I. Formation name, geographic location, architectural element
Upper Omingonde Formation; Farm Omingonde; CH1channel deposit
II. Texture
A. Grain size and sorting
- *20-200 µm*
- *moderately sorted*

B. Grain shape
- *20% subrounded & 80% subangular*

C. Stage of textural maturity
- *mature*

D. Fabric
- *flat lying mica plates, subangular & subangular quartz grains*
- *matrix : grains 70 : 30 => grain supported*
- *grains very closely packed: point contacts (20%) & concavo-convex contacts (80%)*
- *50% depositional porosity* (i.*e. pore-filling cement plus current porosity)*

III. Mineral composition
Grains:
1. Percentage of quartz: 80%
   - *monocrystalline 100% vs. polycrystalline 0%*
   - *undulatory 80% vs. non-undulatory 20%*
   - *grain size 50 µm (30%) & 150 µm (70%)*
2. Percentage of mica: 10%
   - *muscovite & biotite*
   - *grain size 0.5-200 µm*
3. Percentage of other terrigenous minerals: 10 %
   - *pyroxene*
   - *grain size 50-100 µm*

IV. Diagenetic features
- *calcium carbonate cement 70%*
- *Haematite present as blebs & crystals*

V. Classification
- *siltstone*

Sample OMI 4

I. Formation name, geographic location, architectural element
Upper Omingonde Formation; Farm Omingonde; CH4 channel deposit
II. Texture
A. Grain size and sorting
- *0.5-2 mm*
- *well sorted*

B. Grain shape
- *subrounded (10%)& subangular (90%)*

C. Stage of textural maturity
- *immature*

D. Fabric

- *matrix : grains 2 : 98 => grain supported*
- *grains very closely packed: point contacts (20%)* & *concavo-convex contacts (80%)*
- *2% depositional porosity* (i.*e. pore-filling cement plus current porosity)*

III. Mineral composition

Grains:

1. Percentage of quartz: 95%
   - *monocrystalline 100% vs. polycrystalline 0%*
   - *undulatory 80% vs. non-undulatory 20%*
   - *grain size 0.5 mm (10%)* to *1.5 mm (90%)*
2. Percentage of mica: <1%
   - *muscovite*
   - *grain size 0.5-1.5 mm*
3. Percentage of other terrigenous minerals: 5%
   - *feldspar, plagioclase*
   - *grain size 0.5-1.5 mm*

IV. Diagenetic features

- *calcite cement <2%*
- *zircon crystals*

V. Classification

- *sandstone*